Ore Geology Reviews 86 (2017) 673–691

Contents lists available at ScienceDirect

Ore Geology Reviews

journal homepage: www.elsevier.com/locate/oregeo

Geochemical and isotopic evidence for a magmatic-hydrothermal origin of the polymetallic vein-type Zn-Pb deposits in the northwest margin of Jiangnan Orogen, South China

Zhengbing Zhou [a,b], Hanjie Wen [a,b,*], Chaojian Qin [a], Ling Liu [c]

[a] State Key Laboratory of Ore Deposit Geochemistry, Chinese Academy of Sciences, Guiyang 550081, China
[b] University of Chinese Academy of Sciences, Beijing 100049, China
[c] Geological Party 101, Guizhou Bureau of Geology and Minerals Exploration & Development, Kaili 556000, China

ARTICLE INFO

Article history:
Received 31 August 2016
Received in revised form 1 March 2017
Accepted 3 March 2017
Available online 24 March 2017

Keywords:
Polymetallic vein-type Zn-Pb deposits
Indium-bearing ores
Magmatism
Xiangxi–Qiandong metallogenic Zn-Pb belts
South China

ABSTRACT

Polymetallic vein-type Zn-Pb deposits are located in the Xiangxi–Qiandong zinc-lead metallogenic belt (XQMB) of the northwestern margin of the Jiangnan Orogen, South China. Ores are mainly found in fault-bounded quartz veins hosted in the upper part of the Banxi Group that consists of low-grade metamorphic sandstone, siltstone with minor tuff interbeds. The Zn-Pb deposits primarily contain sphalerite, galena, chalcopyrite and pyrite, accompanied by quartz and minor calcite. Zinc, lead, copper, indium and gallium are enriched in these ores. Investigation of the ore fluid reveals low temperature (87–262 °C) with scattered salinity (range from 2.73 to 26.64 wt% $NaCl_{eqv.}$). Hydrogen and oxygen isotopic compositions of fluid inclusions in quartz indicate mixing of magmatic hydrothermal fluid and meteoric water ($\delta^{18}O_{H2O\ SMOW}$ = 0.2‰ to 4.2‰; $\delta D_{H2O\ SMOW}$ = −126‰ to −80‰). Carbon and oxygen isotopic composition of carbonate samples indicate the magmatic hydrothermal origin of CO_3^{2-} or CO_2 in ore-forming fluid ($\delta^{13}C_{PDB}$ = −6.9‰ to −5.7‰, $\delta^{18}O_{SMOW}$ = 11.3‰ to 12.7‰). Sulfur and lead isotopic compositions ($\delta^{34}S_{VCDT}$ = 8.8–14.2‰ and $^{206}Pb/^{204}Pb$ = 17.156–17.209, $^{207}Pb/^{204}Pb$ = 15.532–15.508, $^{208}Pb/^{204}Pb$ = 37.282–37.546) demonstrate that sulfur sources were relatively uniform, and low radiogenic lead isotopic compositions indicate that ore metals were derived from a relatively unradiogenic source, probably by mixing of mantle with crust. Therefore, polymetallic vein-type Zn-Pb mineralization in this area probably arose from a magmatic-related hydrothermal system, and the deposition of sulfides occurred in response to cooling and boiling of magmatic hydrothermal fluids (high salinity, high $\delta^{18}O_{H2O}$ and δD_{H2O} and metal-bearing), and is mainly the result of emplacement into open space and mixing with meteoric water (low salinity, low $\delta^{18}O_{H2O}$ and δD_{H2O}). This study provides direct evidence that magmatism was involved in the ore-forming processes of the low temperature metallogenic district, South China, and it raises awareness about the presence of polymetallic vein-type Zn-Pb deposits in the northwest margin of Jiangnan Orogen and their potential as a source of zinc, copper, indium and gallium.

1. Introduction

South China contains a large and economically significant sediment-hosted Zn-Pb mineralized district that has been subjected to multiple tectonic events since the Archaean. The Xiangxi-Qiandong (western Hunan to eastern Guizhou) Zn-Pb metallogenic belt (XQMB) is located between the Yangtze and Cathaysia Blocks, where the northwest margin of Jiangnan Orogen extends. Its geological setting and mineralization make it important not only in the rock record, but also in terms of reconstructing the metallogeny and tectonic episodes in South China.

Numerous Zn-Pb showings have been described from the XQMB, and two main types of Zn-Pb mineralization have been distinguished; (1) Mississippi valley-type (MVT) and (2) polymetallic vein-type. The MVT deposits are hosted within dolostones or limestones of middle Cambrian to early Ordovician age, and were recognized as the products of the Guangxi Orogeny between the Yangtze and Cathaysia Plates (Schneider et al., 2002; Ye et al., 2005, 2012; Chen et al., 2010; Cai et al., 2014; Tang et al., 2013; Li et al., 2014). The orebodies are stratabound, stratiform and lenticular, and several MVT Zn-Pb deposits have been explored, with major deposits including Huayuan, Xiunao, Dupin, Longjinjie and

* Corresponding author at: State Key Laboratory of Ore Deposit Geochemistry, Chinese Academy of Sciences, Guiyang 550081, China.
E-mail address: wenhanjie@vip.gyig.ac.cn (H. Wen).

http://dx.doi.org/10.1016/j.oregeorev.2017.03.022
0169-1368/

Niujiaotang. The polymetallic vein-type mineralization addressed here occurs in Neoproterozoic sandstone-siltstone, and typical representatives of such are exposed in the folded basement (Fig. 1). The ore bodies are fault-bounded and vein-like, with veins consisting of quartz, calcite and dolomite with locally contain Zn-, Pb- and Cu- sulfides. Economically and particularly, the polymetallic vein-type is by far more important, it is notable that the Zn, Pb, and Cu ores are also enriched with In, Cd and Ga.

Research in the XQMB has mainly focused on its geological features, mineralization, fluid inclusion and geochemistry of the MVT Zn-Pb deposits (Schneider et al., 2002; Ye et al., 2005, 2012; Cai et al., 2014; Tang et al., 2013; Li et al., 2014), with only very limited work having been published about the polymetallic vein-type deposits. These works have mainly focused on providing the initial geologic framework for the deposits (Liu et al., 2008; Yue and Yang, 1993; Yang et al., 2015), and some researchers have attributed the occurrence of the polymetallic vein-type to the presence of MVT deposits, based on their spatial relationships (Figs. 1 and 2; Liu et al., 2008; Yue and Yang, 1993). However, the main gangue mineral in this ore district is quartz and the vein-like mineralization is fault-bounded, which is not consistent with MVT ores that mainly show intergrowth with calcite-bitumen and are strata-bound in middle Cambrian to lower Ordovician sequences. In addition, the indium contents of the polymetallic vein-type ores are markedly higher than that in the of MVT Zn-Pb ores. These features suggest that the polymetallic vein-type deposits are different from those of typical MVT deposits in this district. The metallogenic fluid features, metal sources, and the genesis of the polymetallic vein-type deposits remain unclear.

In this paper we report data that pertain to the geology, fluid inclusions and C-H-O-S-Pb isotopic compositions of the polymetallic vein-type deposits in the XQMB, and provide insight into concerning the mineralizing fluids and metal sources, as well as the mechanism of mineralization. Based on these data, the possibility of magmatic hydrothermal fluid involvement in the ore-forming process is discussed, which appears to be critical for the understanding of ore formation processes in the low temperature metallogenic district of South China.

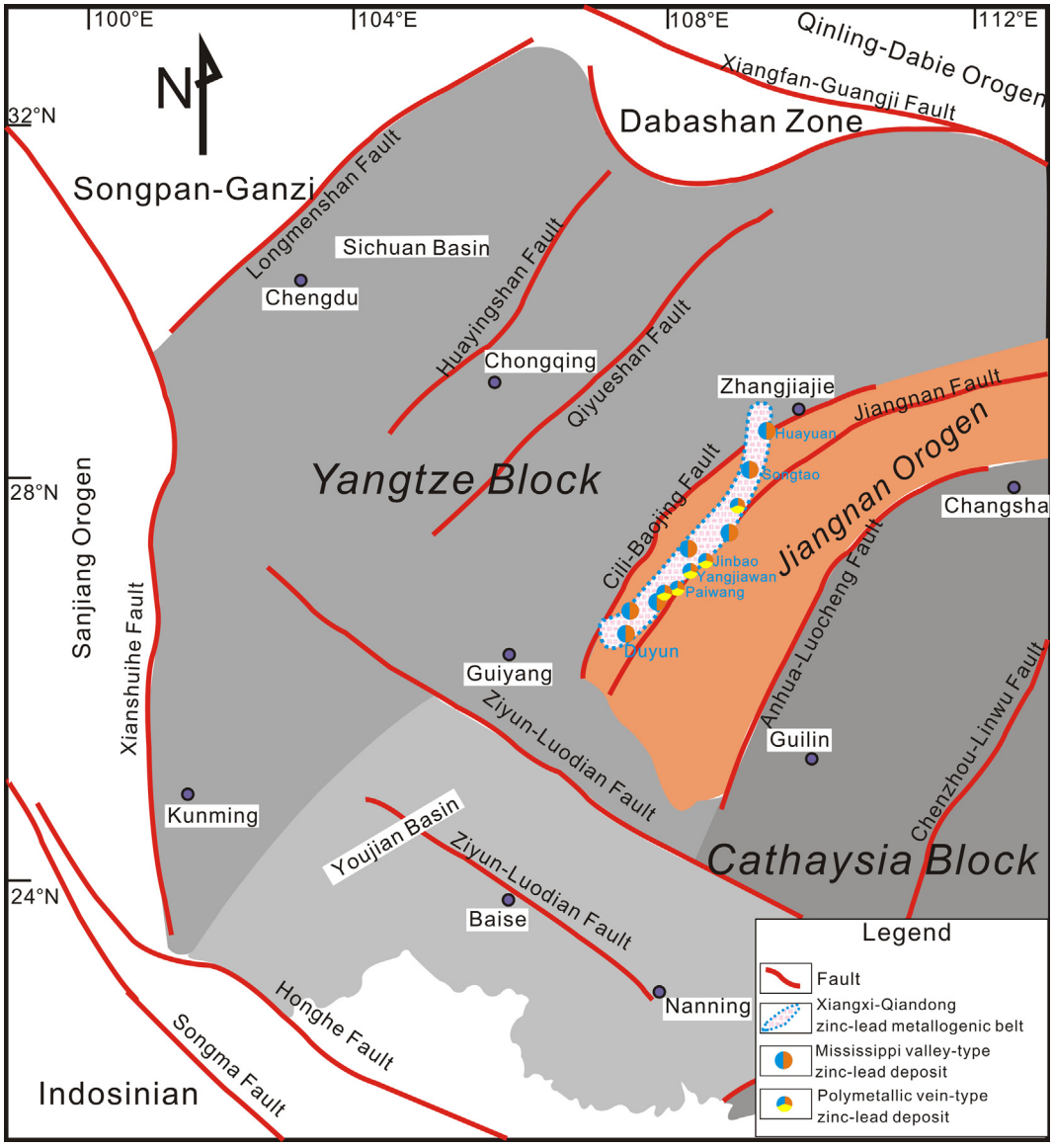

Fig. 1. Regional geological setting and the location of Xiangxi-Qiandong metallogenic belt, showing the location of major zinc-lead deposits. (modified from Wang et al., 2012).

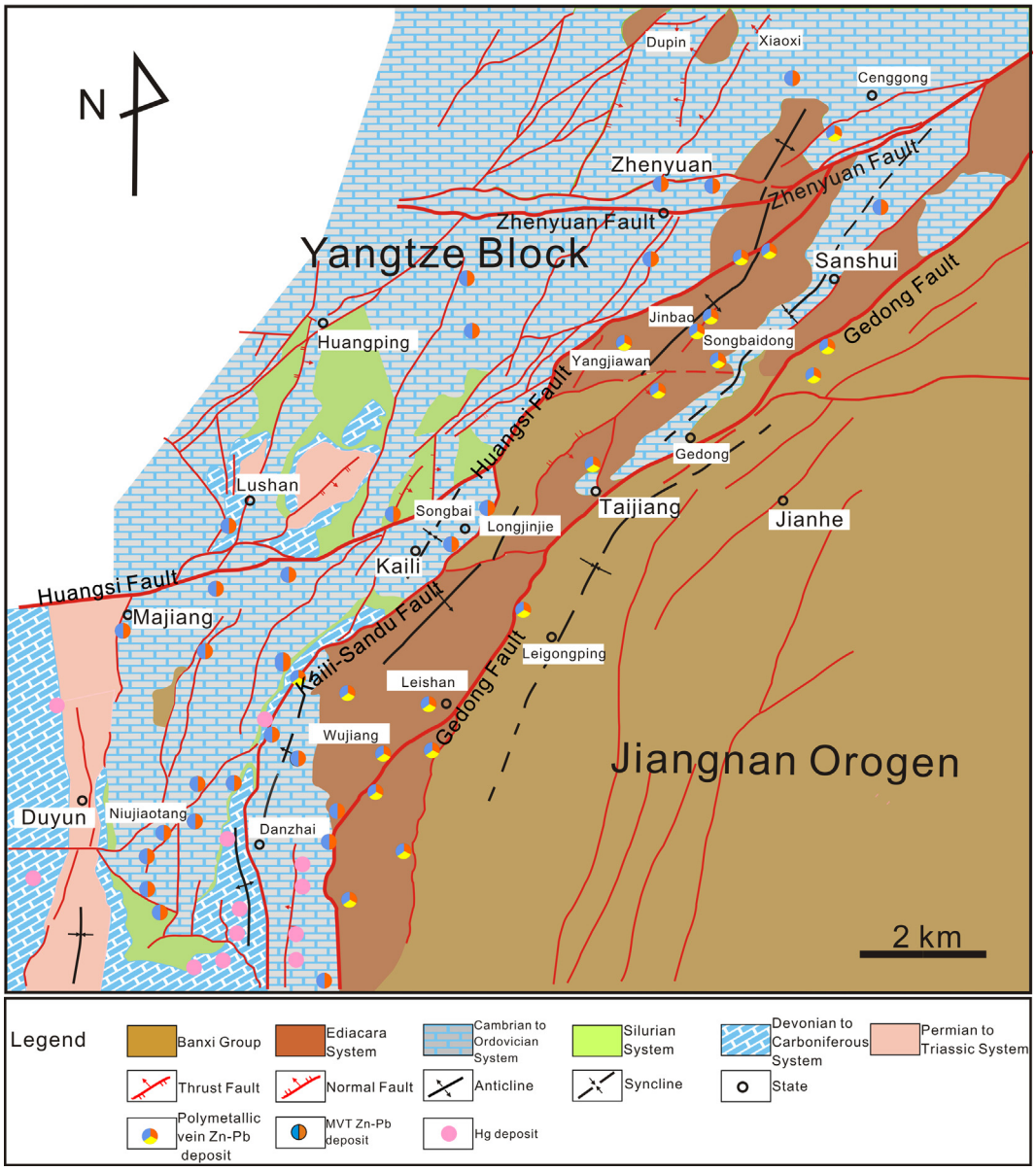

Fig. 2. Map of west-central part of the Xiangxi-qiandong metallogenic belt showing the location of zinc-lead deposits and other sulfide deposits. (modified from Liu et al., 2008).

2. Regional geologic setting

The Jiangnan Orogen in central South China extends for nearly 3000 km and is separated by the Yangtze Block to the north and the Cathaysia Block to the south (Figs. 1 and 2). It is an intracontinental orogenic belt with multi-phase orogenic events from the Neoproterozoic, Paleozoic and Mesozoic. The Jiangnan Orogen was formed by subduction of the paleo-Huanan oceanic lithosphere beneath both the southeastern margin of the Yangtze Block and the northwestern margin of the Cathaysia Block in the period 970 Ma–825 Ma, and then by collisional amalgamation along the two overriding continental margins that combined together at the end of the Jinning Orogeny (ca. 825–815 Ma) (Li et al., 1999, 2003; Zhao and Cawood, 2012; Zhang et al., 2013). The South China Plate broke off in the Neoproterozoic (ca. 800–600 Ma), resulting in the Nanhua rift along the Jiangnan Orogen (Yao et al., 2012). The Nanhua rift was ended by the Guangxi intracontinental orogeny (ca. 540–405 Ma), which allowed for second collision of the Yangtze and Cathaysia Blocks and a final reunion with the South China Plate (Charvet et al., 2010; Shu, 2012; Zhang et al., 2013; Chen et al., 2010, 2012; Wang et al., 2013). During the Variscan period (ca. 405–270 Ma), the South China Plate was relatively stable and characterized by neritic to littoral facies sediments, with local sag zones along major faults (Zhang et al., 2013; Chen et al., 2010). The Indosinian collision then occurred along the Jiangnan Orogen between ca. 270 and 208 Ma (Zhang et al., 2013; Wang et al., 2013).

The northwest margin of the Jiangnan Orogen is underlain mainly by metasedimentary and, to a lesser extent, by glacial sediments and dolostone. Most outcrops in this area are Precambrian basement rocks, which consist of crystalline basement and folded basement rocks. The crystalline basement consists of Archean and Paleoproterozoic metamorphic complexes, comprising upper amphibolite-granulite facies volcanic and sedimentary rocks

(Zhai, 2013). The folded basement rocks are represented by Lengjiaxi and Banxi Groups, the former containing mainly greenschist-facies sandstone, siltstone and slate with minor tuff, spilite, keratophyre, komatiitic rock and associated mafic-ultramafic dykes (Wang et al., 2004, 2008; Zhao and Cawood, 2012). These sequences are characterized by high-angle upright folds and chevron folds overprint. The Banxi Group consists of low-grade metamorphosed sandstone, siltstone with minor tuff interbeds (Wang et al., 2008; Zhao and Cawood, 2012; Zhai, 2013; Geng, 2015). The deformation of the Banxi Group appears to have been weaker than the underlying Lengjiaxi Group, but more intense than overlying sequences. Polymetallic vein-type Zn-Pb occurrences are hosted by rocks of the upper Banxi Group, with successions similar to flysch sediments accumulated in the Nanhua rifts.

From the margin of the Jiangnan Orogen westward to the Yangtze Block, the basement is covered by Neoproterozoic to lower Mesozoic carbonate and siliciclastic successions similar to passive margin sediments accumulated on the southeast flank of the Yangtze Block. These cover sequences start with glacial sediments deposited as the supercontinent of Rodinia broke-up during 800–720 Ma (Zhang et al., 2013). The Changan and Nantuo Formations, consisting of a suite of marine glacial sediments, continental glacial sediments and glacial debris (Yin et al., 2003; Chu, 2004; Huang et al., 2007; Zhang et al., 2008, 2009; Zhou et al., 2004), that correspond to the Sturtian and Marinoan glaciations in the Cryogenian period (Zhang et al., 2008, 2009). The Datangpo Formation, bounded by the Changan Formation and Nantuo Formation, consists of interglacial sediments and manganese-bearing carbonates. Ediacaran sediments that overlie the Nantuo Formation mainly consist of dolomite with minor shale/chert intervals and hydrothermal exhalative sediments (Mao et al., 2002; Jiang et al., 2003; Chen et al., 2009; Huang et al., 2011; Wen et al., 2011; Zhang et al., 2013). Cambrian and Ordovician sediments are characterized by a suite of passive continental margin sediments consisting of carbonaceous mudstone, limestone and sandstone. Silurian sedimentary rocks are filling the basin became folded and uplifted to form the Jiangnan Orogen, followed by Devonian to Permian strata consisting neritic to littoral facies limestone and clastic rocks. Lower Triassic to Jurassic rocks mainly consists of fluvial and lacustrine facies mud and sandstone.

Major structural deformations in this region are closely associated with the tectonic events between the Yangtze and Cathaysia Block, and include the Jinning, Guangxi (Caledonian), Yenshan and Himalaya. The Jinning Orogeny (ca. 825 Ma to 815 Ma) is marked by folding and metamorphism of sediments in the Lengjiaxi Group (Zhao and Cawood, 2012; Zhang et al., 2013). The Guangxi Orogeny (ca. 540–405 Ma) resulted in an intracontinental orogenic environment at this area (Chen et al., 2010; Shu, 2012; Zhang et al., 2013). During the Indosinian Orogeny (ca. 270–208 Ma), this region uplifted to form a continental environment (Zhang et al., 2013; Wang et al., 2013).

Compared to the central and eastern Jiangnan Orogen, magmatic activity in this region is scarce, and only a few lamproites (ca. 503–438 Ma) were intruded into Cambrian sedimentary rocks (Fang et al., 2002; Mei et al., 1998). In fact, the Jinning, Guangxi and Indosinian Orogenies were marked by igneous activity in South China, with three episodes of magmatism having been distinguished: (1) ca. 820 Ma granite and diabase, such as the Motianlin, Yuanbaoshan and Sanfang plutons (Li et al., 2012; Shu, 2012; Yao et al., 2012); (2) ca. 400–464 Ma (centralized in ca. 420–446 Ma) and (3) ca. 220–233 Ma granites, such as the Baimashan and Yuechenlin plutons (Wang et al., 2012, 2013; Yang et al., 2014; Wu et al., 2012; Chen et al., 2013). Those magmatic activities, especially the latter two, were accompanied by the formation of numerous W, Sn, Mo, Cu, Zn and Pb deposits (Hu and Zhou, 2012).

3. Geology and mineralogy of polymetallic vein-type zinc-lead deposits

3.1. Deposit geology

Polymetallic vein-type Zn-Pb deposits are clustered in the XQMB, which is located at the conjunction of the Yangtze Block and Jiangnan Orogen (Figs. 1 and 2). Active mines are located in the Jinbao metallogenic district (Aihe, Bengchong, Laodu and Pingmen deposits), the Nansun metallogenic district (Nansun and Paiwang deposits), and the Yangjiawan and Miaoniao deposits.

The lithologies exposed in mineralized areas are Neoproterozoic to Cambrian in age and are shown in Figs. 2 and 3. The rocks in descending order are: the Neoproterozoic Banxi Group, which predominantly consists of low-grade metamorphosed sandstone, siltstone and minor tuff, with a maximum thickness of 7000 m; the Neoproterozoic Nanhua and Ediacaran Systems, which are composed of glacial to interglacial sediments and micrite; and the Early Cambrian System, which contains micrite or algae-bearing dolostone and limestone. Polymetallic vein-type Zn-Pb ore is mainly hosted in the upper part of Banxi Group.

These deposits are fault-bounded and controlled by the NE-trending Shidongkou fault zone (Figs. 2 and 4). The deposits

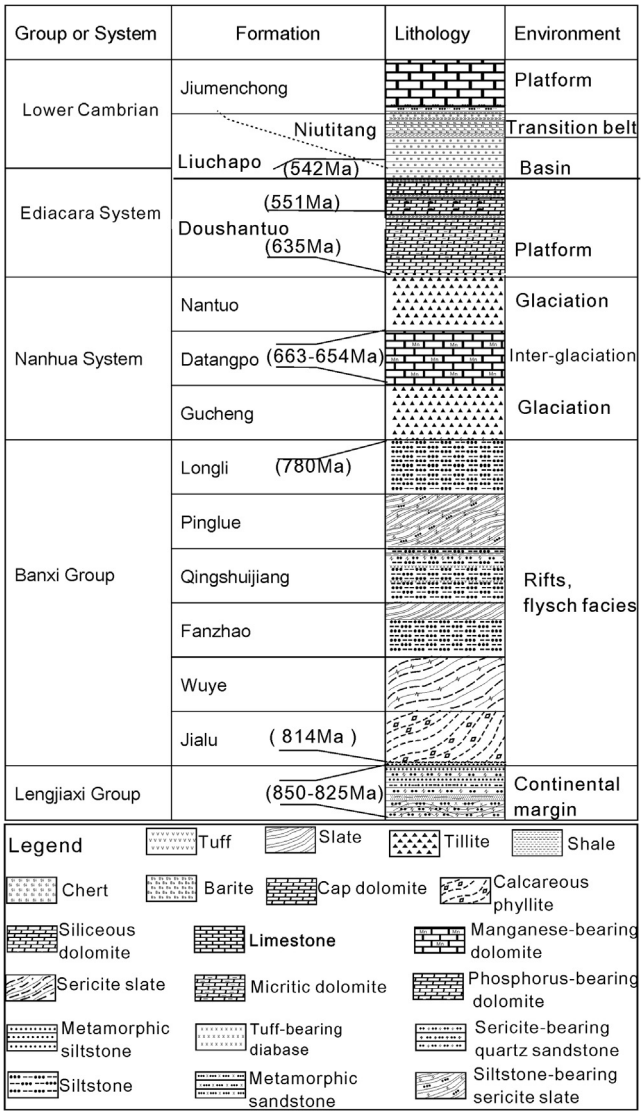

Fig. 3. Summary stratigraphy of the Xiangxi-Qiandong metallogenic belt.

occur as quartz veins and sulfide breccias that are distributed irregularly throughout the XQMB. Individual veins are typically 3–400 cm in width and up to tens of meters in strike length, although a few large veins occur that are up to 7 m wide and 325 m long. The larger ore veins are always irregular, tend to pinch and swell, whereas the smaller veins are uniform with infilling of interlayers or subsidiary fissures of adjacent faults. Both veins types have sharp boundaries against host rocks (Fig. 4). All the known sulfide-bearing veins are associated with normal faults, particularly where they cut the fold axes of anticlines are the optimum mineralization sites.

Major fold structures in this area, from northwest to southeast, include the Rongshan anticline, Guigai syncline and Panshan anticline. Dominant faults in the area include Mandong, Shidongkou and Taijiang faults, which are subsidiaries faults of the large Baojin-Tongren-Kaili fault system. Ore-bearing faults and folds are NE to NNE-trending (N30° E to N80°E strike), and fold limbs are characterized by low dip angles (10°–30°) and faults have high dip angle (55°–75°).

3.2. Wall rock alteration, ore mineralogy and paragenesis

Host rock is predominantly brecciated with silicification, minor pyritic and carbonate alteration. This hydrothermal alteration is mainly developed on both sides of ore veins with silicification predominantly and closely associated with mineralization (Fig. 5c–f). Sphalerite, galena, pyrite and chalcopyrite are the principal sulfide minerals in the relatively simple mineral assemblage that exists, and tetrahedrite and bornite occur only in minor amounts in most of the deposits. Quartz and calcite are the major gangue minerals, along with minor amounts of sericite. The amount of calcite increases in areas with relatively higher hydrothermal fluids emplacement site.

The mineralization is generally massive and vein-like, with some breccia textures. Quartz precipitated prior to sulfides is always found crystallized around the breccia fragments of host rocks, while the sulfides infill vugs and interstices in the quartz, resulting in sulfides preferentially forming massive assemblages and nodules in the ore veins (Figs. 5a–f and a–e). Some comb-like textures are present in the quartz (Fig. 5d), and was likely caused by pulses and changes in silica saturation in the hydrothermal systems (Seifert and Sandmann, 2006; Sinclair et al., 2006). Under polarized light microscopy, sphalerite crystals sometimes have zonal texture with reddish brown coloration in the core and bright yellow at the rim (Fig. 6c/d). The zonal texturing is thought to reflect a non-uniform ore fluid composition (Zn, Cd, and Fe) during sphalerite crystallization (Cook et al., 2009; Ye et al., 2011).

Under reflected light microscopy, lamellar and micro-veined chalcopyrite appears to be distributed in double-crystal joints and cracks of sphalerite (Fig. 6g–i). This assemblage is different from the 'chalcopyrite disease', which is characterized by vermicular chalcopyrite inclusions in sphalerite (Barton and Bethke, 1987;

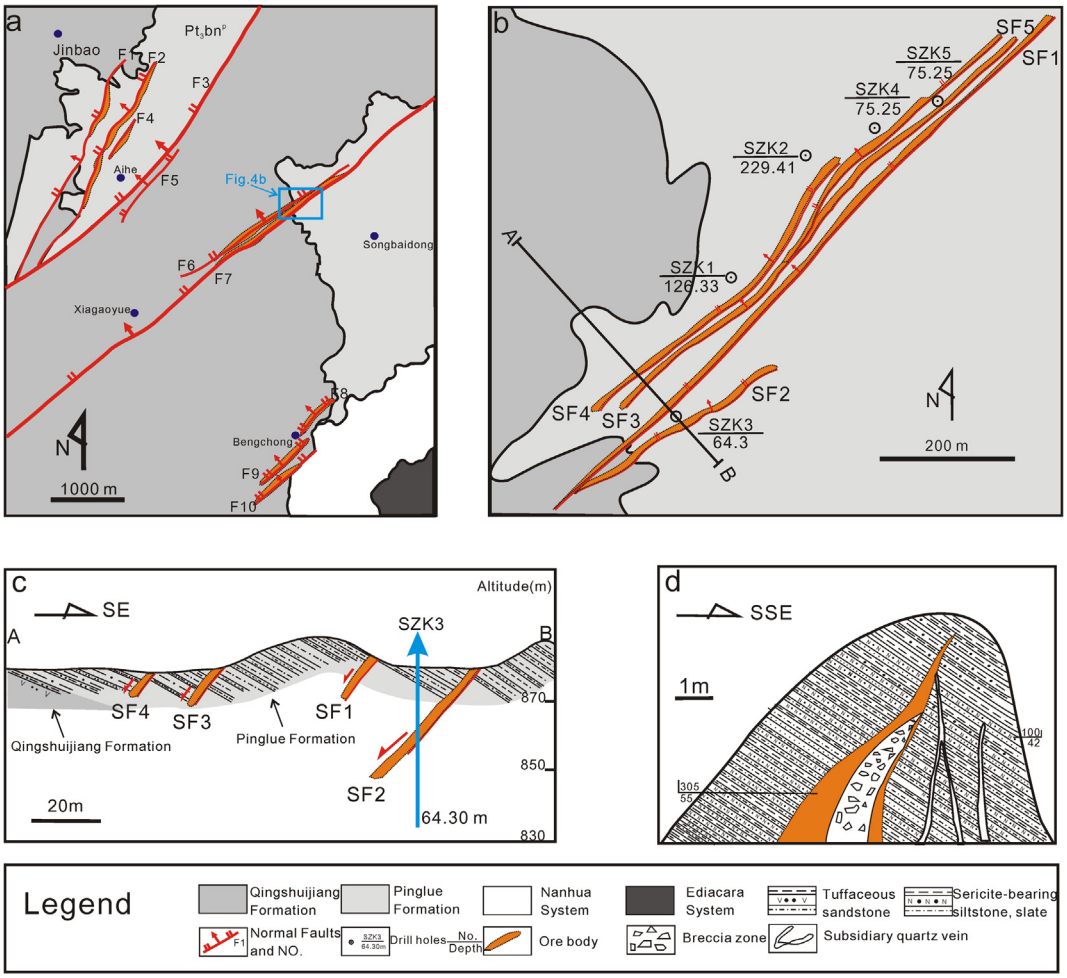

Fig. 4. Geological map of Jinbao metallogenic district **(a)** and the Songbaidong deposit in the central of Jinbao metallogenic district **(b)**, line AB is the location of cross-section shown on (c); **(c)** the cross-section through Songbaidong deposit, showing mineralization of typical zinc-lead polymetallic vein-type deposits in Xiangxi-Qiandong metallogenic belt; and **(d)** cross section sketch of an individual ore vein.

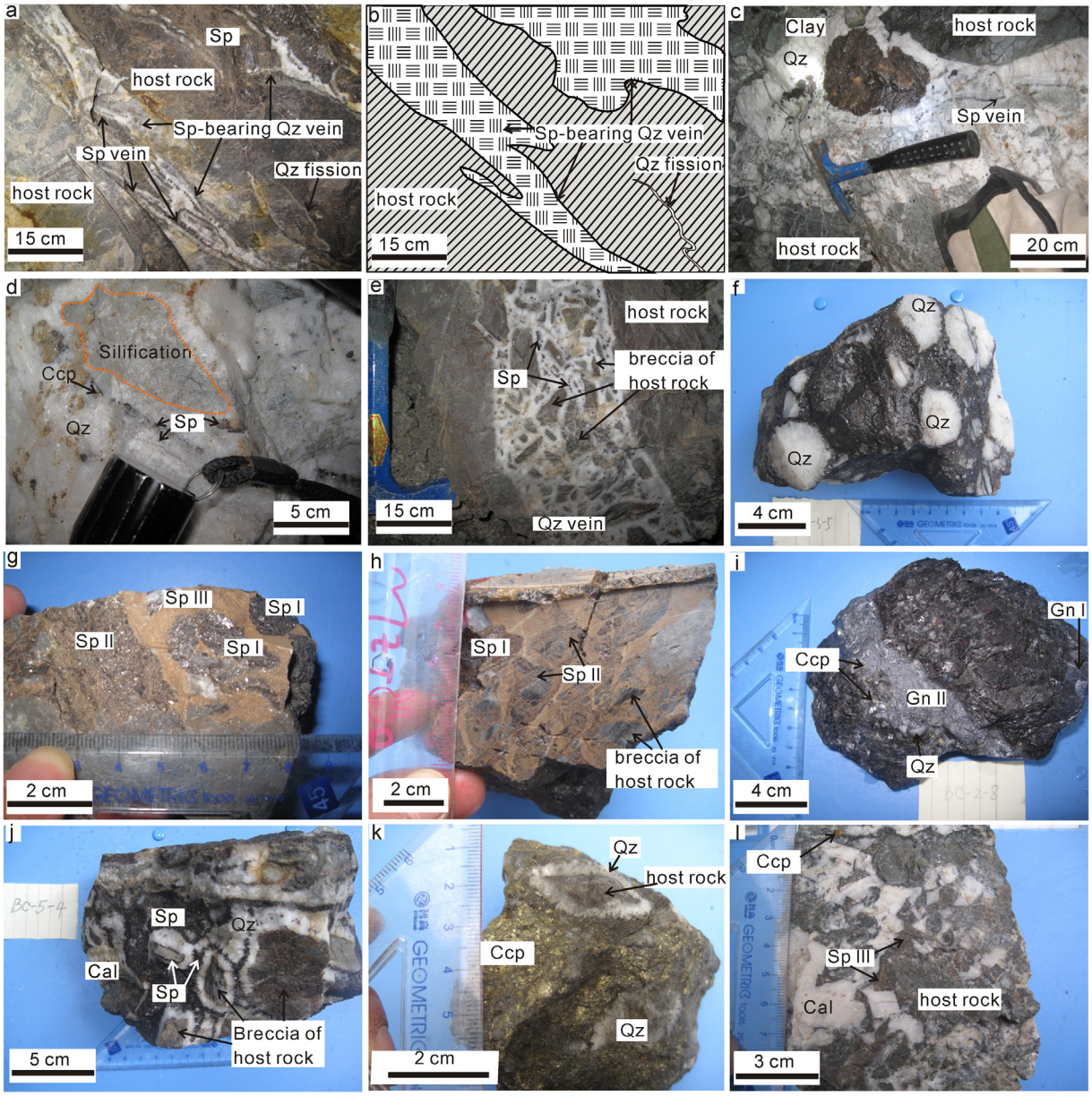

Fig. 5. Examples of metal-bearing veins and ores from the Xiangxi-Qiandong metallogenic belt. (a) and (b) Ore veins fill in the fracture of host rock. (c) Massive and vein-like sphalerite in quartz veins; ore veins with sharp boundaries against host rock. (d) Layers of comb-textured quartz and sphalerite. (e) Hydrothermal breccia of host rock. (f) Quartz and sphalerite nodules. (g) and (h) Sphalerite generations. (i) Fine-grained galena cross cut coarse sphalerite. (j) Quartz crystallized around breccia/fragments of host rocks and with sulfides filling in the vug and interstitial of quartz, minor chalcopyrite grains distributed in sulfide veins. (k) Massive chalcopyrite assemblage. (l) Massive sulfides intergrowth with calcite. Abbreviations: *Qz* quartz; *Sp* sphalerite; *Gn* galena; *Ccp* chalcopyrite; *Cal* calcite.

Eldridge et al., 1988), but rather occurs as chalcopyrite in massive (Fig. 5k), lamellar or micro vein-like shapes (Fig. 6g–i), in sphalerite. This suggests a texture caused by replacement, and not exsolution. Hydrothermal fluids were evidently enriched in copper and iron in the late-ore stage, probably caused by the copper and iron becoming concentrated during ore-forming processes, or by the influx of fluids already rich in copper and iron.

Based on the extensive textural and mineralogical associations observed in the deposits, the mineralization process has been classified into four stages (Fig. 7): (1) Pre-ore stage; (2) Main ore stage; (3) Late ore stage; and (4) Post sulfide stage. In the Pre-ore stage, euhedral granular quartz crystallized around host rock breccia and filled interstices in the host rocks. This quartz typically forms encrustations on breccia fragments of host rocks, with minor amounts of pyrite and sphalerite precipitated in intergranular porosity. In the Main ore stage, a complex polymetallic sulfide assemblage coprecipitated with quartz and calcite, dominated by coarse grained, subhedral–euhedral granular black sphalerite, coarse grained galena and pyrite (Fig. 5f/g/i/j). Intergranular pores and spaces in the quartz and calcite were infilled by main stages sulfides (sphalerite, galena, and pyrite) (Fig. 5f–j). Sulfides also infilled residual vuggy porosity of earlier quartz generations, with resulting veins typically displaying drusy crystal growth and similar encrustations. The Late ore stage is represented by fine-grained sphalerite and galena coprecipitated with fine grained quartz and minor calcite, showing pale-yellow to light brown colors in hand specimen (Figs. 5j–i and 6c/e). Parts of the earlier stage sulfide and host rock were brecciated and cemented at this time by late-

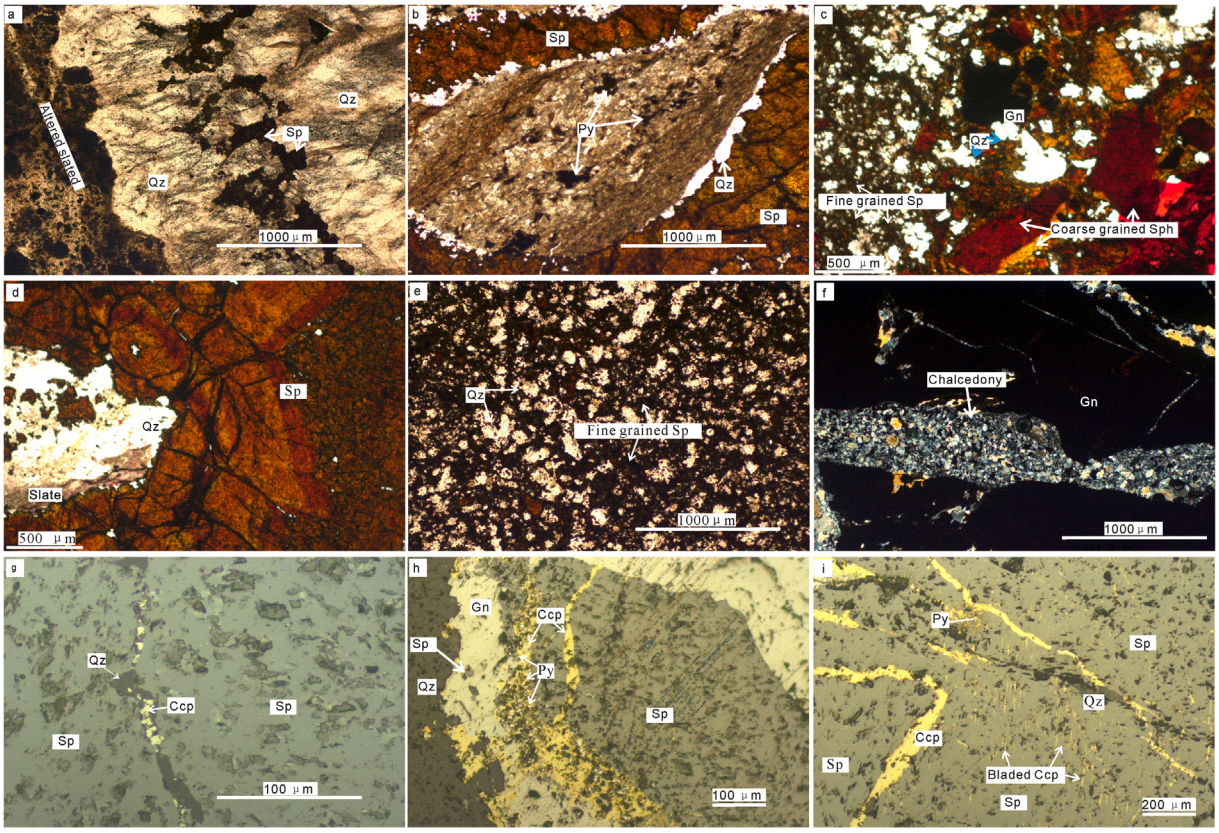

Fig. 6. Photomicrographs of samples collected from the polymetallic vein-type zinc-lead deposits, Xiangxi-Qiandong metallogenic belt. (a) Quartz crystallized around breccia/fragments of host rocks, like an encrustation of fragment; sphalerite occurs interstitial to quartz. (b) Sphalerite crystallized as encrustation in quartz. (c) Early stage sphalerite breccia cemented by fine-grained quartz and sphalerite. (d) Zoned texture of sphalerite. (e) Fine-grained sphalerite coprecipitated with fine-grained quartz. (f) Early stage galena cut by chalcedony veins. (g) Chalcopyrite and quartz veins fill in the fracture of sphalerite. (h) Chalcopyrite, galena and pyrite replacing sphalerite. (i) vein-like and bladed chalcopyrite distributed in the fracture and double-crystal joint of sphalerite. Photomicrograph a-f were taken under transmitted plane-polarized light, g-i were taken under reflected plane-polarized light. Abbreviations: *Qz* quartz; *Sp* sphalerite; *Gn* galena; *Ccp* chalcopyrite; *Py* pyrite.

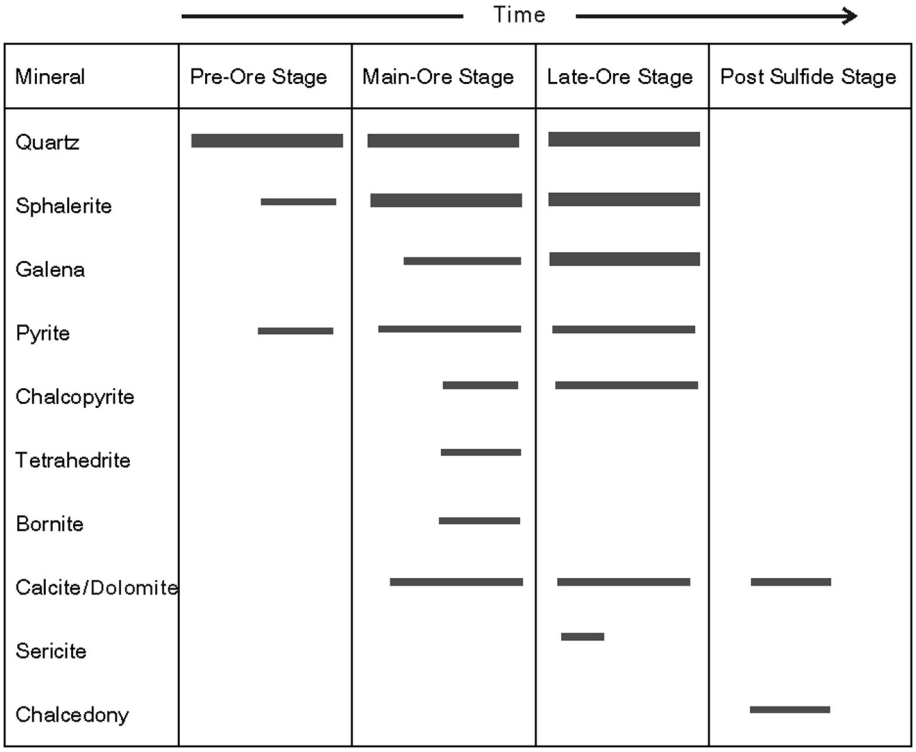

Fig. 7. Simplified paragenetic sequence of ore and gangue minerals from the Polymetallic vein-type Zn-Pb deposits.

stage minerals (Figs. 5j–i and 6c/e). Lastly, minor amounts of chalcedony and calcite veins cross-cut the earlier generations of minerals during the Post sulfide stage.

4. Samples and methodology

The texture and paragenetic studies of minerals were based on field observations as well as the investigations on hand specimens and under microscope. In order to investigate the characters of ore-forming processes, samples were collected from the Jinbao metallogenic district, Nansun, Paiwang and Yangjiawan deposits. Represented samples were crushed to 40–80 mesh, to selected sulfides and carbonates and quartz by handpicked base on a binocular microscope. And then crush these sulfides and carbonate sample to 200 meshes under an agate mortar.

Fluid inclusion petrography, microthermometric measurements and the composition analysis of single fluid inclusion were carried out at the State Key Laboratory of Ore Deposit Geochemistry (SKLODG), Institute of Geochemistry, Chinese Academy of Sciences, Guiyang, China. Microthermometric data of fluid inclusions were based on the observation of quartz and calcite built upon observed phase transitions of fluid inclusions at -196 to 600 °C with a Linkam THMSG-600 heating-freezing stage, coupled with a Zeiss microscope. For freezing runs, the precision is ±0.1 °C for ice melting; for heating runs, the precision is ±0.5 °C for critical point. Salinity expressed as weight percent NaCl eqv. (wt% $NaCl_{eqv.}$) was calculated from microthermometric data, using the equations provided by Bodnar (1993). The compositions of single fluid inclusion were measured by Renishaw inVia Reflex Raman microprobe with an argon ion laser source of 514 nm. The scanning range of spectra was set between 100 cm^{-1} and 4300 cm^{-1} with an accumulation time of 60 s for each scan; the width of laser beam is 1 μm, and spectral resolution is about 0.14 cm^{-1}. Processes are following the method described by Burke (2001).

Ten quartz samples were selected for hydrogen and oxygen isotope analysis, which are carried out at the Geological Analysis Laboratory, Ministry of Nuclear Industry, Beijing, China. Hydrogen (H_2) is obtained from H_2O was released from fluid inclusions and then reduced with zinc (Coleman et al., 1982). Oxygen is obtained from the reaction of quartz with BrF_5, which is done according to the procedures outlined by Clayton and Mayeda (1963). The evolved H_2 and O_2 gas were measured on a Finnigan™ MAT 251 gas source mass spectrometer (Thermo Fisher Scientific, Waltham, Massachusetts) and isotopic data ($\delta^{18}O$ and δD) are reported in ‰ relative to the Vienna Standard Mean Ocean Water (V-SMOW). Uncertainties at 1σ were estimated to be better than ±0.2‰ for $\delta^{18}O$ and ±2.0‰ for δD.

Thirteen carbonate samples were selected for carbon-oxygen isotope analysis. The carbon and oxygen isotopic compositions of carbonates were measured by an EM-MAT-253 gas source mass spectrometer at SKLODG. The CO_2 obtained from carbonates are reacted with anhydrous phosphoric acid at 72 °C for 12 h using Gas Bench. Evolved CO_2 gas was analyzed on a Finnigan™ MAT 253 gas source mass spectrometer. Isotopic data are reported in ‰ relative to the Peer Dee Belemnite (PDB) for carbon and oxygen. the following standards were used for internal calibration standards: GBW04416 (calcite, $\delta^{13}C_{PDB} = 1.61‰$, $\delta^{18}O_{PDB} = -11.59‰$), GBW04405 (calcite, $\delta^{13}C_{PDB} = 0.57$ ‰, $\delta^{18}O_{PDB} = -8.49‰$), NBS18 (calcite, $\delta^{13}C_{PDB} = -5.01‰$, $\delta^{18}O_{PDB} = -23.2‰$) and L-SVEC (lithium carbonate, $\delta^{13}C_{PDB} = -46.6‰$, $\delta^{18}O_{PDB} = -26.7‰$). The analytical precision at 2σ for $\delta^{13}C$ and $\delta^{18}O$ are ±0.2‰ and ±2.0‰, respectively. The values of $\delta^{18}O_{SMOW}$ were calculated based on the equations of Friedman and O'Neil (1977), where $\delta^{18}O_{SMOW} = 1.03086 \times \delta^{18}O_{PDB} + 30.86$.

Twenty-one sphalerite samples, two pyrite samples, six galena samples and four chalcopyrite samples from the polymetallic vein Zn-Pb deposits, and one sphalerite and galena sample, three pyrite samples from Duping Zn-Pb deposit (a MVT deposit) were prepared for sulfur isotopic analysis. Sulfur isotope analysis was carried out using an EA-MAT-253 mass spectrometer at SKLODG. Sulfides were combusted with copper oxide under vacuum at 1000 °C to produce SO_2 which was used for the gas mass spectrometer measurements (Robinson and Kusakabe, 1975). Isotopic data were reported as $\delta^{34}S$ relative to IAEA-S-1 ($\delta^{34}S_{VCDT} = -0.30‰$), IAEA-S-2 ($\delta^{34}S_{VCDT} = 22.62‰$) and IAEA-S-3 ($\delta^{34}S_{VCDT} = -32.49‰$) standards for sulfur. The relative error at 2σ was better than 0.1‰.

Ten sulfide samples (sphalerite, galena, chalcopyrite and pyrite) and eight host rock samples were selected to measure lead isotopic compositions, which were performed at the Geological Analysis Laboratory, Ministry of Nuclear Industry, Beijing, China, using an IsoProbe-T thermal ionization mass spectrometer. Lead was separated and purified by using conventional cation-exchange technique, with diluted HBr as eluant. Lead isotopes are reported

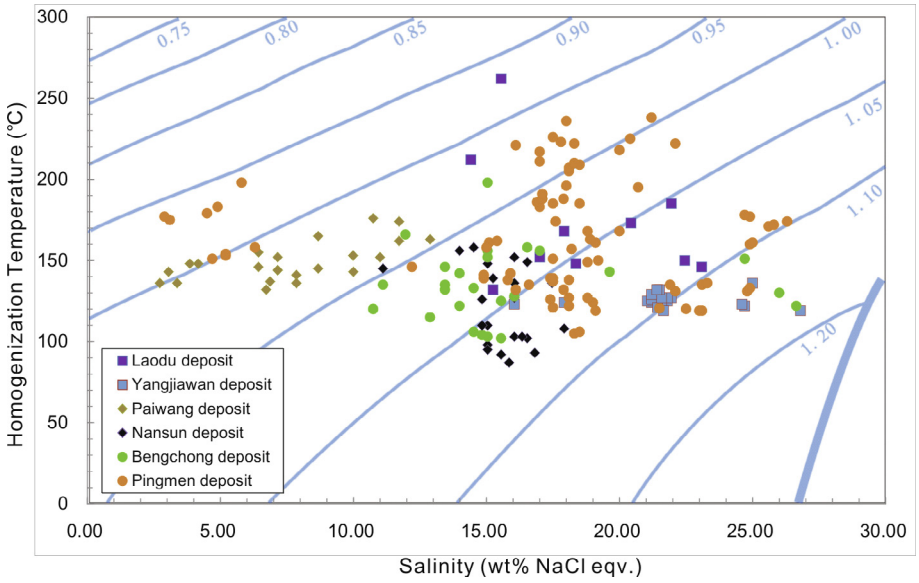

Fig. 8. Summary of T_h, salinity and associated with minimum density of fluids in the polymetallic vein Zn-Pb deposit, the blue lines are isodense line.

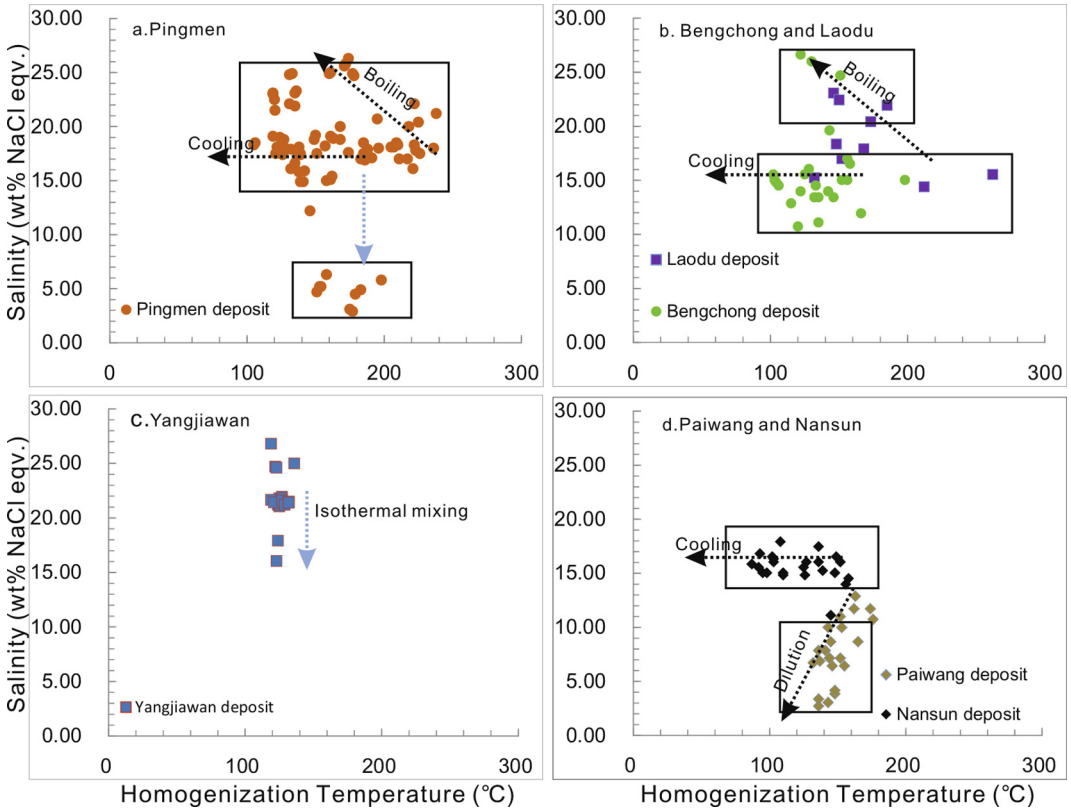

Fig. 9. a/b/c/d is T_h vs. salinity of fluids in Pingmen, Bengchong, Yangjiawan and Nansun-Paiwang deposits, respectively. The dotted line with arrow represents the assumed fluid evolution processes.

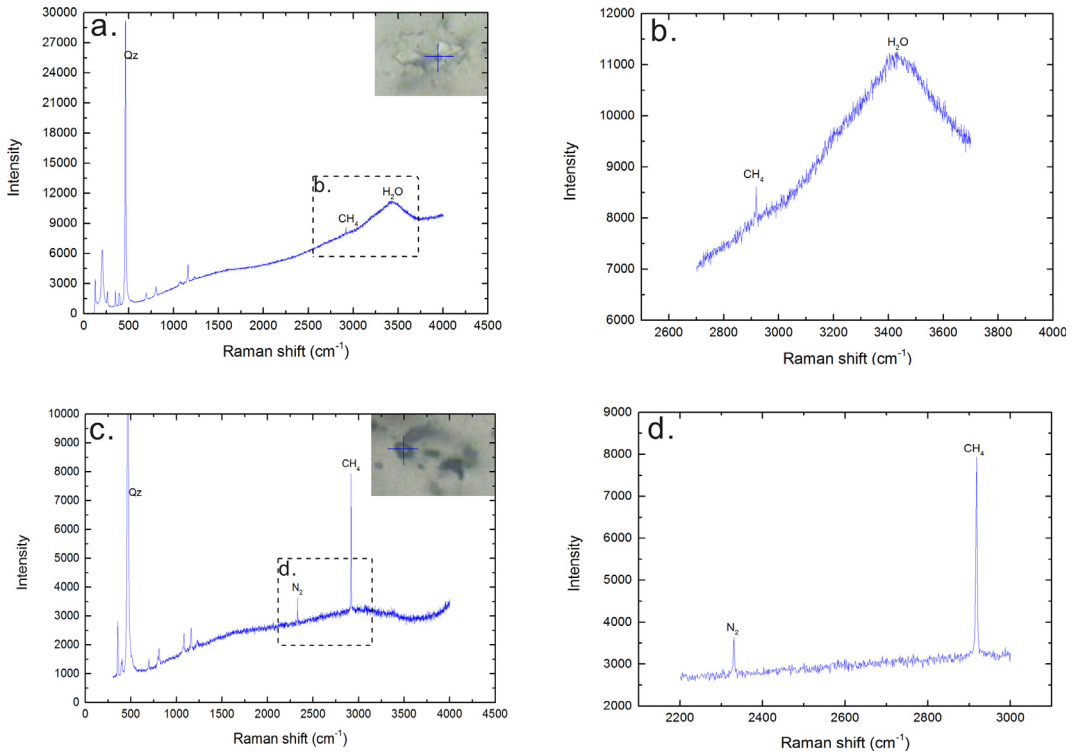

Fig. 10. Representative Raman spectra of fluid inclusions in the polymetallic vein-type Zn-Pb deposit. (a,b) H_2O- and CH_4-spectrum of vapor phase in fluid inclusion; (c,d) CH_4- and N_2-spectrum of vapor phase in CH_4-dominated fluid inclusion.

Table 1
Summary of aqueous fluid inclusion data for the polymetallic vein-type deposits and Longjinjie MVT zinc-lead deposit.

Deposit	Mineral	Type	Number	Tm/clath-ice (°C)	Tm (°C)	Salinity (wt% NaCleqv.)
Laodu	Quartz	Polymetallic vein	16	−21.3 to −11.1 (−15.2)	132–262 (172)	14.42–23.09 (18.64)
Yangjiawan	Quartz	Polymetallic vein	21	−19 to −9.6 (−17.1)	119–132 (126)	13.55–21.95 (20.36)
Nansun	Quartz	Polymetallic vein	26	−14 to −7.5 (−11.5)	87–190 (127)	11.1–17.92 (15.54)
Paiwang	Quartz	Polymetallic vein	33	−9 to −1.6 (−4.8)	132–183 (150)	2.73–12.88 (7.66)
Bengchong	Quartz	Polymetallic vein	30	−26 to −7.2 (−12.3)	102–198 (133)	10.74–26.64 (15.80)
Pingmen	Quartz	Polymetallic vein	83	−1.7 to −25.4 (-14.5)	105–238 (164)	2.9–26.3 (17.6)
Longjinjie	Calcite	MVT	12	−19.3 to −16 (−18.1)	78–161 (132)	19.63–22.16 (21.29)

Table 2
Oxygen and hydrogen isotopic data for fluid in quartz from polymetallic vein-type deposits.

Sample No.	Location	δD_{H2O} (‰)	$\delta^{18}O_{Quartz}$ (‰)	$\delta^{18}O_{H2O}$ (‰)
BC-2-2	Bengchong	−111	14.8	1.0
BC-2-3	Bengchong	−112	14.0	0.2
BC-3-1	Bengchong	−103	14.9	1.1
BC-3-2	Bengchong	−116	14.5	0.7
BC-3-3	Bengchong	−124	14.8	1.0
BC-3-4	Bengchong	−126	14.7	0.9
2 BC-5-kd-1	Bengchong	−122	15.2	1.4
PM-2	Pingmen	−84	15.4	3.7
PM-1-14	Pingmen	−84	15.3	3.6
PM-1-10	Pingmen	−80	15.9	4.2

Note: $\delta^{18}O_{H2O} = \delta^{18}O_{Quartz} - 3.38 \times 10^6/T^2 + 3.4$ (Clayton et al., 1972).

relative to the measured ratio of NBS981 and corrected for instrument mass fractionation. The precision of $^{208}Pb/^{206}Pb$ measurements (1 μg of Pb) is better than 0.005%.

5. Results

5.1. Fluid inclusions

Fluid inclusions trapped in quartz during the main mineralization stage vary in size from 3 to 10 μm, which is most abundant with minor amounts exceeding 10 μm in size. These fluid inclusions have two phases (liquid + vapor) with the vapor phase ranging from 5 to 10 vol% of the whole inclusion (Fig. 10). They always have negative crystal distribution and rounded shape. The majority of fluid inclusions measured in this quartz could represent the characters of the hydrothermal fluids, owing to the earlier and later stage quartz which are typically milky and chalcedony in which trapped fluid inclusions are too small to precisely observe the phase transitions under the microscope. Quantity of CH_4 and H_2O, and minor amount of N_2 had been observed in vapor phase of fluid inclusions by means of the Raman microprobe.

Upon freezing these inclusions formed a brown, granular ice at about −74 to −42 °C (mean = −59 °C). First ice melting was observed in a single inclusion at −44 °C. Last ice melting occurred between −1.6 °C and −26 °C, corresponding to salinities of 2.73–26.64 wt% $NaCl_{eqv.}$ according to the equations of Bodnar (1993) (Table 1; Figs. 8 and 9; Electronic Appendix A). Inclusions are homogenized into liquid phase between 78 and 262 °C.

5.2. Hydrogen and oxygen isotopic compositions

The hydrogen and oxygen isotopic compositions of the analyzed ore fluids are shown in Table 2 and Fig. 11. The $\delta^{18}O_{H2O}$ values are calculated based on oxygen isotope fractionation factors between quartz and water where: $1000\ln\alpha = 3.38 \times 10^6/T^2 - 3.40$ (Clayton et al., 1972), and temperature (T) involved in calculation is based on the homogenization temperature of fluid inclusions from corresponding deposits. The $\delta^{18}O_{H2O}$ and δD_{H2O} values range from 0.2 to 4.2 ‰ and −126 to −80 ‰, respectively.

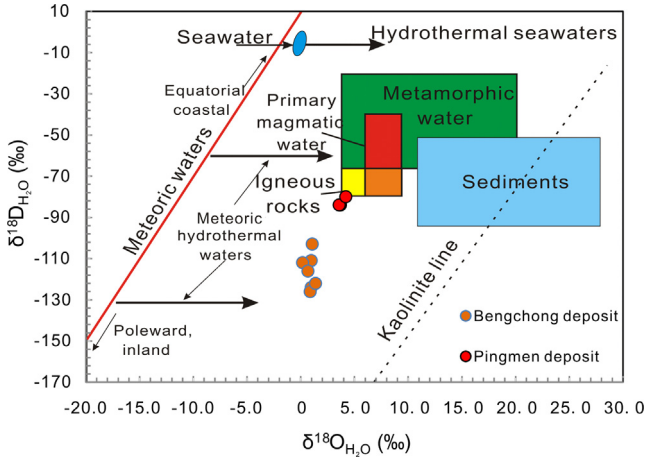

Fig. 11. $\delta 18O_{H2O}$ vs. $\delta 18O_{H2O}$ diagrams of the polymetallic vein zinc-lead deposits. The range of the meteoric water line, kaolinite line and different materials including igneous rocks, primary magmatic water, sediments and metamorphic water were modified from Hoefs (2009) and Ohmoto (1986).

5.3. Carbon and oxygen isotopic compositions

The carbon and oxygen isotopic compositions of carbonates in the polymetallic vein-type and MVT deposits are listed in Table 3 and Fig. 12. Carbonate samples of the polymetallic vein-type deposits demonstrated that $\delta^{18}O_{SMOW}$ values are ranging from 11.2 to 12.7‰ (n = 18, mean = 11.9 ± 0.4‰) and $\delta^{13}C_{PDB}$ are ranging from −6.9 to −5.7 ‰ (n = 18, mean = -6.2 ± 0.8‰). Carbonate samples from MVT zinc-lead deposits had $\delta^{18}O_{SMOW}$ ranging from 14.6 to 23.9 ‰ (n = 15, mean = 14.6 ± 2.5‰) and $\delta^{13}C_{PDB}$ ranging from −3.6 to 2.1 ‰ (n = 15, mean = −9.1 ± 4.8‰).

5.4. Sulfur isotopic compositions

The $\delta^{34}S_{VCDT}$ values of sulfides (sphalerite, galena, pyrite and chalcopyrite) selected from polymetallic vein Zn-Pb deposit are listed in Table 4 and range from 8.8 to 14.2‰ with an average value

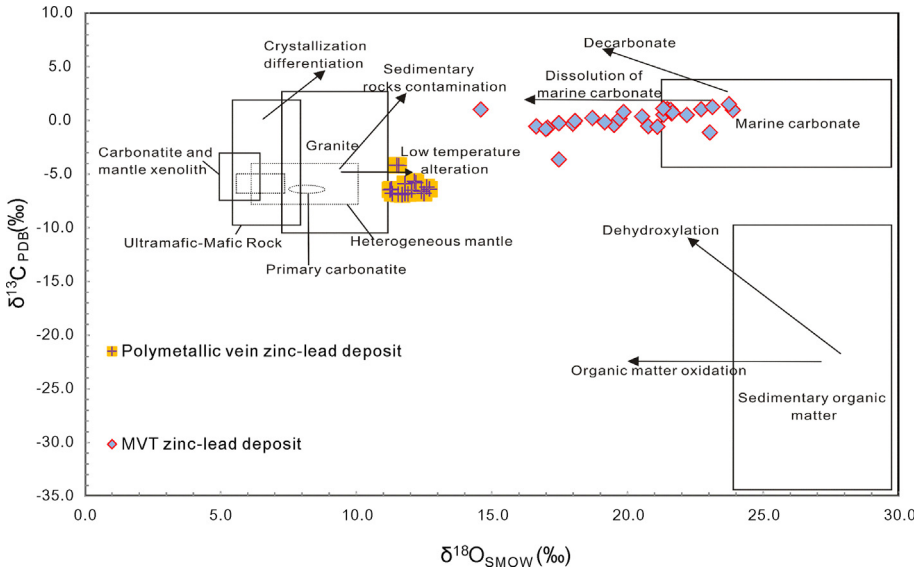

Fig. 12. $\delta^{18}O_{SMOW}$ vs. $\delta^{13}C_{PDB}$ plots for carbonate samples in the Xiangxi-Qiandong zinc-lead metalogic belt.

Table 3
Oxygen and carbon isotopic data for carbonate samples from the Xiangxi-Qiandong zinc-lead metallogenic belt.

Sample No.	Minerals	$\delta^{18}O_{PDB}$ (‰)	$\delta^{13}C_{PDB}$ (‰)	$\delta^{18}O_{SMOW}$ (‰)	Deposit	Remarks
BC-x-1	Dolomite	−17.9	−6.6	12.4	Bengchong	Polymetallic vein
BC-x-2	Dolomite	−17.8	−6.8	12.5	Bengchong	Polymetallic vein
BC-x-3	Dolomite	−17.6	−6.4	12.7	Bengchong	Polymetallic vein
BC-x-4	Calcite	−17.7	−6.2	12.6	Bengchong	Polymetallic vein
JP20	Calcite	−18.2	−5.7	12.1	Bengchong	Polymetallic vein
BC-x-6	Calcite	−18.1	−5.8	12.2	Bengchong	Polymetallic vein
PM-x-1	Calcite	−18.5	−5.9	11.8	Pingmen	Polymetallic vein
PM-x-4	Calcite	−18.5	−6.8	11.8	Pingmen	Polymetallic vein
ah2	Calcite	−19.0	−6.5	11.3	Aihe	Polymetallic vein
ah1	Dolomite	−18.6	−6.9	11.7	Aihe	Polymetallic vein
AH-x-1	Dolomite	−19.0	−6.4	11.3	Aihe	Polymetallic vein
ah3	Dolomite	−19.0	−6.8	11.3	Aihe	Polymetallic vein
AH-x-3	Dolomite	−18.6	−6.9	11.7	Aihe	Polymetallic vein
PW-6	Calcite	−16.8	−131	13.6	Paiwang	Polymetallic vein
YJW-5	Calcite	−18.4	−6.8	11.9	Yangjiawan	Polymetallic vein
YJW-6	Dolomite	−18.7	−4.2	11.6	Yangjiawan	Polymetallic vein
YJW-6-gray	Dolomite	−18.8	−4.2	11.5	Yangjiawan	Polymetallic vein
2LD-3-3-1	Dolomite	−18.7	−6.9	11.6	Laodu	Polymetallic vein
2LD-3-3-2	Dolomite	−18.3	−6.5	12.0	Laodu	Polymetallic vein
ZXB4	Dolomite	−11.3	2.1	19.2	Xiaoxi	MVT
DP01	Dolomite	−12.2	−0.1	18.3	Duping	MVT
LM_2*	Calcite	1.11	−9.25	21.32	Huayuan	MVT
LM-3*	Calcite	1.26	−7.5	23.13	Huayuan	MVT
LM-5*	Calcite	1.5	−6.91	23.74	Huayuan	MVT
LM_15*	Calcite	1.01	−15.78	14.59	Huayuan	MVT
SZS-8*	Calcite	−0.31	−12.48	17.99	Huayuan	MVT
SZS-16*	Calcite	−0.04	−12.41	18.07	Huayuan	MVT
SZS-27*	Calcite	−1.12	−7.59	23.04	Huayuan	MVT
ST-15*	Calcite	−0.26	−12.99	17.47	Huayuan	MVT
ST-17*	Calcite	−0.41	−11.01	19.51	Huayuan	MVT
ST-20*	Calcite	0.22	−11.79	18.71	Huayuan	MVT
PKC-2*	Calcite	0.51	−8.41	22.19	Huayuan	MVT
PKC-3*	Calcite	0.16	−10.82	19.71	Huayuan	MVT
PKC-8*	Calcite	−0.17	−11.35	19.16	Huayuan	MVT

Note: $\delta^{18}O_{SMOW} = 1.03086 \times \delta^{18}O_{VPDB} + 30.86$ (Friedman and O'Neil, 1977).
The sample number with superscripts * means these data were cited from Cai et al., 2014, the others were from this study.

of 12.6 ± 1.4‰ (n = 34). Sulfide samples record a narrow range of $\delta^{34}S_{VCDT}$ values, i.e., 10.9–14.4‰ (n = 22, mean = 13.1 ± 0.8‰) for sphalerite, 8.7–10.7 ‰ (n = 6, mean = 10.1 ± 0.7‰) for galena, 12.9–14.2 ‰ (n = 4, mean = 13.7 ± 0.6‰), 13.0-13.4 ‰ (n = 2, mean = 13.2 ± 0.3‰) for pyrite. The ranges of $\delta^{34}S_{VCDT}$ values of sulfides selected from MVT Zn-Pb deposit range from 25.0 to 34.1‰ (n = 20, mean = 29.5 ± 3.0‰).

5.5. Lead isotopes

Lead isotopic compositions of sulfides and host rocks from the polymetallic vein Zn-Pb deposits in this study together with those of the basement rocks, lamproite and MVT zinc-lead deposits from XQMB are summarized in Table 5 (full data in Electronic Appendix B) and shown in Fig. 14.

Table 4
Sulfur isotope of sulfide samples from the Xiangxi-Qiandong zinc-lead metallogenic belt

Sample No.	Mineral	Sample types	$\delta^{34}S$ (‰)	Location
PW-12	Galena	Coarse-grained	8.8	Paiwang
PW-13	Sphalerite	Black, coarse-grained	13.8	Paiwang
NS-1	Sphalerite	Brownish black	13.6	Nansun
NS-2-1-a	Sphalerite	Brownish black	13.3	Nansun
NS-2-1-b	Galena	Coarse-grained	10.4	Nansun
NS-4-2	Sphalerite	Black	13.2	Nansun
NS-7-b	Pyrite		13.0	Nansun
NS-6-a	Sphalerite		10.9	Nansun
PM-2	Sphalerite	Black, coarseegrained	13.7	Pingmen
PM-1-4	Galena	Fine-grained	10.7	Pingmen
PM-1-9	Sphalerite	Black, coarseegrained	13.6	Pingmen
PM-1-14	Sphalerite	Black, coarse-grained	14.3	Pingmen
PM-1-16	Sphalerite	Brownish black	12.9	Pingmen
JP16	Chalcopyrite		13.7	Pingmen
JP17	Chalcopyrite		12.9	Pingmen
JP18	Chalcopyrite		14.2	Pingmen
JP19	Chalcopyrite		13.9	Pingmen
YJW-1-a	Pyrite		13.4	Yang jiawan
YJW-1	Sphalerite		13.0	Yang jiawan
YJW-2	Sphalerite	Brownish, black-reddish brown	12.1	Yang jiawan
YJW-6	Sphalerite	Brownish black-reddish brown	12.1	Yang jiawan
BC-2-2-a	Sphalerite	Black, coarseegrained	12.7	Bengchong
BC-2-8-b	Galena	Coarse-grained	10.0	Bengchong
BC-2-8-c	Galena	Fine-grained	10.0	Bengchong
BC-2-8-a	Sphalerite	Black-maroon, coarse-grained	12.7	Bengchong
BC-3-5-a	Sphalerite	Black, coarse-grained	14.4	Bengchong
BC-3-5-b	Sphalerite	Fine-grained	13.7	Bengchong
BC-3-kd-2	Sphalerite	Black, coarse-grained	13.3	Bengchong
BC-5-1-a	Sphalerite	Black, coarse-grained	12.9	Bengchong
BC-5-1-b	Galena		10.6	Bengchong
BC-5-4-a	Sphalerite	Black, coarse-grained	13.2	Bengchong
BC-5-4-b	Sphalerite		13.5	Bengchong
2LD-3-3	Sphalerite	Black-brown	12.7	Laodu
AH4	Sphalerite		11.5	Aihe
DP02	Pyrite	MVT	27.4	Duping
DP-kd	Galena	MVT	25.0	Duping
DP-4-a	Sphalerite	MVT	27.5	Duping
DP-4-b	Pyrite	MVT	28.2	Duping
DP-3	Pyrite	MVT	26.3	Duping
SZS-01*	Galena	MVT	26.8	Huayuan
SZS-02*	Sphalerite	MVT	31.3	Huayuan
SZS-05*	Sphalerite	MVT	31.7	Huayuan
SZS-08*	Sphalerite	MVT	31.8	Huayuan
SZS-10*	Sphalerite	MVT	34.1	Huayuan
SZS-15-2*	Sphalerite	MVT	26.3	Huayuan
SZS-15-3*	Pyrite	MVT	33.0	Huayuan
SZS-16*	Sphalerite	MVT	33.5	Huayuan
SZS-16*	Galena	MVT	26.5	Huayuan
SZS-25*	Galena	MVT	27.2	Huayuan
SZS-26*	Sphalerite	MVT	33.4	Huayuan
SZS-26*	Galena	MVT	27.6	Huayuan
SZS-27*	Sphalerite	MVT	31.8	Huayuan
SZS-27*	Galena	MVT	27.2	Huayuan
SZS-15-2*	Pyrite	MVT	32.8	Huayuan

Note: The sample number with mark of " *" right behind means these data were cited from Cai et al., 2014, the others were from this study.

Sulfides representing the main stages of hydrothermal mineralization in polymetallic vein-type deposits have a range of $^{206}Pb/^{204}Pb$ rations from 17.156 to 17.209 (mean = 17.187), $^{207}Pb/^{204}Pb$ from 15.532 to 15.508 (mean = 15.458), and $^{208}Pb/^{204}Pb$ from 37.282 to 37.546 (mean = 37.371).

The lead isotopic data of the basement rocks in this region show a considerable spread. The ratios of $^{206}Pb/^{204}Pb$,$^{207}Pb/^{204}Pb$, and $^{208}Pb/^{204}Pb$ for the Banxi Group range from 15.528–20.106 (mean = 18.004), 15.430–15.705 (mean = 15.542) and 37.897–41.640 (mean = 39.031), respectively; the ratios of $^{206}Pb/^{204}Pb$, $^{207}Pb/^{204}Pb$, and $^{208}Pb/^{204}Pb$ for the Lengjiaxi Group range from 18.832–22.038 (mean = 19.993), 15.586–15.937 (mean = 15.715), and 39.294–46.917 (mean = 41.870), respectively.

The MVT Zn-Pb deposits have high and heterogeneous radiogenic lead isotopic compositions and show positive correlations of $^{206}Pb/^{204}Pb$ vs. $^{207}Pb/^{204}Pb$ and $^{206}Pb/^{204}Pb$ vs. $^{208}Pb/^{204}Pb$. Sulfides from the MVT Zn-Pb deposits have a range of $^{206}Pb/^{204}Pb$ ratios from 18.028 to 18.293 (mean = 18.173), $^{207}Pb/^{204}Pb$ from 15.524 to 15.875 (mean = 15.721), $^{208}Pb/^{204}Pb$ from 38.099 to 38.888 (mean = 38.373). Limestone and dolostone of Qingxudong formation, have Pb isotopic ratios that are in good agreement with sulfides of the MVT deposits. The ratios of $^{206}Pb/^{204}Pb$, $^{207}Pb/^{204}Pb$

Table 5
Summary of Pb isotopic composition of sulfides, and host rocks in the Xiangxi-Qiandong zinc-lead metallogenic belt

Sample Type	Number of Samples	$^{208}Pb/^{204}Pb$	$^{207}Pb/^{204}Pb$	$^{206}Pb/^{204}Pb$	μ value	T (Ma)
Polymetallic vein-Type zinc-lead deposit						
Pingmen No.1 Vein	3	37.335–37.380 (37.362)	15.452–15.472 (15.463)	17.177–17.196 (17.186)	9.34–9.38 (9.36)	872–893 (884)
Bengmhong No.2 Vein	2	37.282–37.503 (37.393)	15.438–15.508 (15.473)	17.156–17.196 (17.176)	9.32–9.46 (9.39)	878–924 (901)
Bengmhong No.3 Vein	1	37.324	15.443	17.189	9.32	860
Bengmhong No.4 Vein	1	37.319	15.445	17.202	9.32	853
Bengmhong No.5 Vein	2	37.297–37.252 (37.325)	15.432–15.460 (15.446)	17.174–17.188 (17.181)	9.30–9.36 (9.33)	849–889 (869)
Laodu No.3 Vein	1	37.546	15.464	17.209	9.36	869
Aihe	2	37.375–37.488 (37.432)	15.470–15.485 (15.478)	17.139–17.258 (17.199)	9.37–9.42 (9.40)	840–940 (890)
Altered Basement						
Pingmen No.1 Vein	3	37.314–39.410 (38.160)	15.449–15.491 (15.463)	17.157–17.511 (17.300)	9.33–9.36 (9.34)	685–890 (803)
Basement						
Banxi Groups	25	37.897–41.640 (39.031)	15.430–15.705 (15.542)	15.528–20.106 (18.004)	9.24–10.01 (9.43)	–
Lengjiaxi Groups	7	39.294–46.917 (41.870)	15.586–15.937 (15.715)	18.832–22.038 (19.993)	9.39–11.25 (9.82)	–
Lamporite						
Zhen Yuan	3	–	15.299–15.526 (15.378)	17.187–17.709 (17.442)	9.01–9.4 (9.14)	–
MVT zinc-lead deposit						
Huayuan	51	38.099–38.888 (38.373)	15.524–15.875 (15.721)	18.028–18.293 (18.173)	9.33–10.03 (9.73)	157–585 (480)
MVT zinc-lead deposit's Host rock						
Qing Xudong Fm.	12	38.107–39.408 (38.483)	15.479–15.783 (15.665)	17.204–19.073 (18.285)	9.35–9.79 (9.61)	–

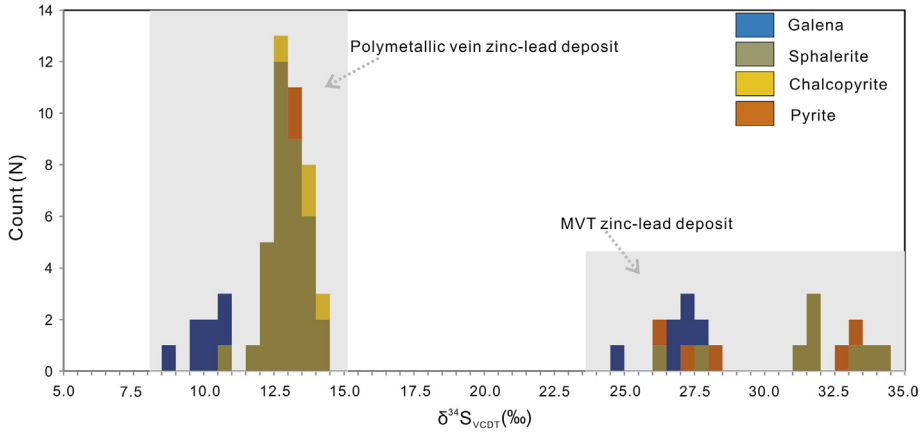

Fig. 13. Histograms of $\delta^{34}S_{VCDT}$ of sulfide minerals from the Xiangxi-Qiandong zinc-lead metallogenic belt.

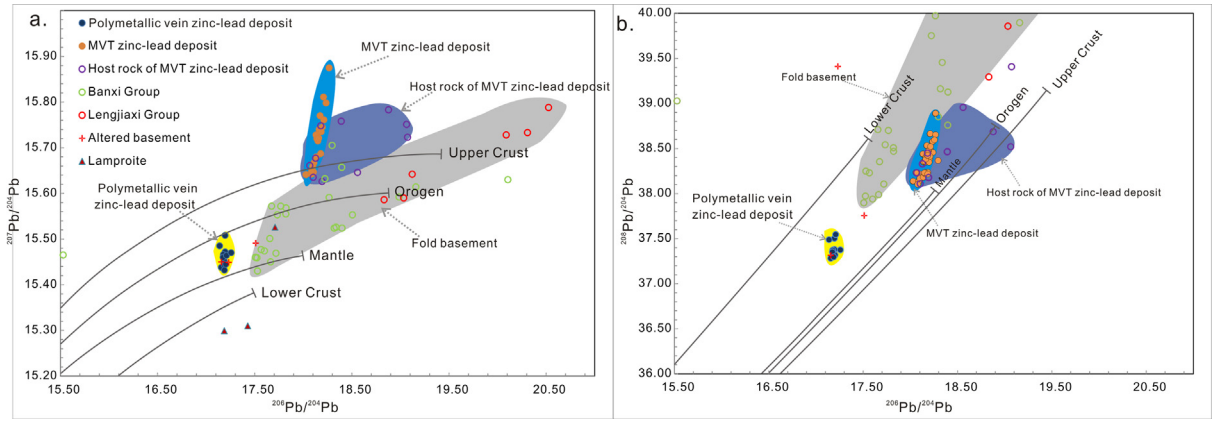

Fig. 14. Plots of **a** $^{206}Pb/^{204}Pb$ vs. $^{207}Pb/^{204}Pb$ and **b** $^{206}Pb/^{204}Pb$ vs. $^{208}Pb/^{204}Pb$ (after Zartman and Doe, 1981) for sulfide minerals and host rocks from the Xiangxi-Qiandong zinc-lead metallogenic belt.

and $^{208}Pb/^{204}Pb$ for Qingxudong formation are in the 38.107–39.408 (mean = 38.483), 15.479–15.783 (mean = 15.665) and 17.204–19.073 (mean = 18.285) ranges, respectively.

6. Discussion

6.1. Nature of ore-forming fluids

Fluid inclusions in quartz from the polymetallic vein Zn-Pb deposits are H_2O-NaCl brines characterized by variable salinity and moderate to low temperature. In the diagram of T_h-salinity plot contoured with lines of constant fluid density, the minimum densities of fluids are mainly in the 0.95–1.10 g/cm^3 (Fig. 8) (Wilkinson, 2001). In T_h vs. salinity diagram, fluid inclusions in quartz from the Pingmen, Bengchong, Yangjiawan and Paiwang-Nansun deposits all show similar homogenization temperature with variable salinity, and can be broadly distinguished into two domains (Fig. 9).

Boiling may have occurred during the ore-forming processes. Fluid inclusion microthermometry and laser Raman spectrometry identified variable amounts of volatiles (mainly CH_4 with minor N_2 and CO_2) in fluids, the Paiwang deposit contains CH_4-dominated inclusions (Fig. 10). Conversely, most fluid inclusions from the polymetallic vein-type deposits are predominantly aqueous and homogenized at similar temperatures, providing further evidence that boiling of ore-forming fluid occurred. The slightly lower salinity/density of fluid inclusions may be related to the dilution of ore-forming fluids by meteoric water.

In the polymetallic vein deposits, ore-forming fluids likely ascended along faults and infilled extensional structures, with cooling and boiling providing effective mechanisms for mineralization. The deposits of Pingmen, Bengchong, Laodu and Nansun show evidence that these ore-forming processes probably underwent cooling and boiling throughout the fluid evolution process (Wilkinson, 2001). The Yangjiawan deposit shows evidence of isothermal mixing tends, while the Paiwang deposit also shows a trend of dilution through the ore-forming process (Wilkinson, 2001) (Fig. 9). Thus, the limited rock volume, boiling and mixing processes provided the crucial conditions for effective ore mineral precipitation in those polymetallic vein-type deposits.

6.2. Sources of ore-forming fluids

Both oxygen and hydrogen isotopic compositions of fluids can systematically change in response to variations of geological processes (Taylor, 1997; Hoefs, 2009; Rye, 1993). The $\delta^{18}O_{H2O}$ values of ore-forming fluids in the Bengchong and Pingmen deposits are in the 0.2–1.4 ‰, and 3.6–4.2 ‰ range, respectively, whereas the δD_{H2O} values vary from −126‰ to −103‰ and −84‰ to −80 ‰, respectively. δD_{H2O} and $\delta^{18}O_{H2O}$ values for samples collected from the Pingmen deposit are close to primary magmatic water composition (Taylor, 1997), and the $\delta^{18}O_{H2O}$ and δD_{H2O} values share a positive correlation.

It can be concluded that the difference and the positive correlation of $\delta^{18}O_{H2O}$-δD_{H2O} values between these two deposits resulted from two different geologic processes, either: (1), the fluid-rock interaction during which the host rocks were critical in controlling oxygen and hydrogen isotopic composition controlling or (2), fluids with high $\delta^{18}O_{H2O}$ and δD_{H2O} values mixing with fluids of relatively lower values.

As mentioned previously, the host rocks are mainly low-grade metamorphosed sandstone, siltstone with minor tuff, thus fluid-rock interaction would increase the $\delta^{18}O_{H2O}$ value of the fluid, but there is mostly a trend of decreasing δD_{H2O} values in the fluid (Yeh, 1980; Suchecki and land, 1983; Moldovanyi et al., 1993). Moreover, these host rocks lack organic matter which is known to decrease the δD_{H2O} value of fluids (Goldfard et al., 2004). However, compared with the amount of hydrogen involved in hydrothermal fluids, the hydrogen concentration in these host rocks is low enough to significantly affect the hydrogen isotopic composition of the fluid (Taylor, 1997; Moldovanyi et al., 1993; Deen et al., 1994). In contrast, the largest difference between the Bengchong and Pingmen deposits, in terms of δD_{H2O} values, is 46‰ and, regardless of whether the $\delta^{18}O_{H2O}$ and δD_{H2O} values of the original ore-forming fluids were high or not, fluid-rock interaction could not lead to such a large difference in δD_{H2O} values and maintain a positive correlation between $\delta^{18}O_{H2O}$ and δD_{H2O} values of ore-forming fluids in this region.

Importantly, the hydrogen and oxygen isotopic compositions of the Bengchong and Pingmen deposits are similar to those of magmatic epithermal Ag-Cu-Pb-W-Bi-Au deposits in Julcani, Peru and magmatic steam alunite Deer Trail Pb-Zn-Ag-Au-Cu manto deposits in Marysvale district, Utah (Rye, 1993; Deen et al., 1994; Beaty et al., 1986). Therefore, such trends could be the result of mixing of fluids with relatively high $\delta^{18}O_{H2O}$ and δD_{H2O} values and fluids with relatively low $\delta^{18}O_{H2O}$ and δD_{H2O} (meteoric water). As the oxygen isotopic compositions of ore-forming fluids in the Pingmen deposit are close to the range of primary magmatic waters, a contribution of magmatic hydrothermal fluid during mineralization cannot be ruled out.

The $\delta^{13}C_{PDB}$ values of carbonate samples collected from the polymetallic vein-type deposits are in a narrow range of −6.9‰ to −5.7‰, similar to mantle carbon isotopic compositions (−5‰ to −7‰, Hoefs, 2009) and within the range of magmatic rocks (−3‰ to −30‰, Hoefs, 2009). The $\delta^{18}O_{SMOW}$ values of carbonate samples from the polymetallic vein-type deposits are in the 11.2 ‰–12.7‰ range, which is slightly higher than that of magmatic rocks. In the diagram of $\delta^{18}O_{SMOW}$ vs. $\delta^{13}C_{PDB}$ (Fig. 12), samples from polymetallic vein-type deposits plot tightly within or near the igneous fields and parallel with the direction of low temperature alteration of igneous rocks. Hence, the CO_3^{2-} or CO_2 in the ore-forming fluids of the polymetallic vein-type deposits were predominantly derived from a magmatic hydrothermal system.

The carbon and oxygen isotopic compositions of carbonate samples from the polymetallic vein-type deposits are strongly distinguishable from those collected from the MVT deposits of the XQMB or contiguous areas of the Sichuan-Yunnan-Guizhou zinc-lead metallogenic district. Carbonate samples collected from the MVT deposits have consistent $\delta^{13}C_{PDB}$ and depressed $\delta^{18}O_{SMOW}$ values and plot within-near the marine carbonate field in the diagram of $\delta^{18}O_{SMOW}$ vs. $\delta^{13}C_{PDB}$ (Fig. 12). This suggests that the CO_3^{2-} or CO_2 in the ore-forming fluids were mainly derived from the dissolution of marine carbonate (Spangenberg et al., 1996; Leach et al., 2005; Ye et al., 2012).

Based on both hydrogen oxygen and carbon isotopic compositions it can be asserted that the ore-forming fluids are closely related to igneous activity in the area, and suggest that the ore-forming processes may have operated by reactions of relatively high $\delta^{18}O_{H2O}$, δD_{H2O} and high salinity magmatic hydrothermal fluids being channeled into open spaces along fault zones and mixing with low $\delta^{18}O_{H2O}$, δD_{H2O} and salinity fluids, such as meteoric water.

6.3. Sources of ore metals

Ore minerals from the polymetallic vein deposits chiefly consist of sphalerite, galena, pyrite and chalcopyrite, and no sulfate minerals occur. Thus, in the hydrothermal system, H_2S is the dominant sulfur species or the hydrothermal fluid is under a lower redox state than the SO_2/H_2S boundary. This suggests that the sulfur isotopic composition of sulfides can represent the total sulfur isotopic compositions of the hydrothermal fluid ($\delta^{34}S_{\Sigma S} \approx \delta^{34}S_{\ sulfide}$)

(Ohmoto, 1972; Hoefs, 2009; Kelly et al., 1979). The $\delta^{34}S_{VCDT}$ values of selected sulfide minerals vary from 8.8 ‰ to 14.2 ‰ (n = 34, mean = 12.6 ± 1.4‰), which is lower than that of the MVT deposits in the XQMB (Fig. 13).

In sediment-hosted Zn-Pb deposits, the sulfur sources are most typically from connate water trapped in host rocks, seawater, or paleo oil-field brine (Leach et al., 2005; Machel et al., 1995; Li and Zhang, 2012; Wu et al., 2013). Formation water and seawater must undergo thermochemical sulfate reduction (TSR) or bacterial sulfate reduction (BSR) to reduce sulfates to hydrosulfides, and then complexing with base metal ions such as Zn^{2+} and Pb^{2+} (Machel et al., 1995; Leach et al., 2005; Cai et al., 2003). Nevertheless, sulfate minerals are scarce in the host rocks, and BSR/TSR processes will result in a varied sulfur isotope fractionation between sulfides and the parent sulfates. This principally depends on the system being open or close, the physicochemical conditions and the rates of sulfate supply (Machel et al., 1995). In natural geological processes, it is difficult for such a narrow sulfur isotopic composition to result from low-temperature sulfate reduction processes. Also, no organic matter or sulfate minerals were found in the ores or host rocks, neither in hand species nor under the microscope. Thus, it is highly unlikely that the host rocks and seawater were the direct sulfur source for the polymetallic vein deposits.

Another possibility is that base metal bearing-hydrothermal fluids migrated upwards and then mixed with H_2S-dominated paleo-oil-field brine. This possibility can be discounted; however, because: (a) no organic substances such as bitumen could be found in the ores either in hand specimens or under the microscope; and (b) the $\delta^{34}S_{VCDT}$ values of bitumen in the Majiang paleo-oil-field brine reservoir ($\delta^{34}S_{VCDT}$ = 22.6‰ to 26.2‰; Ye et al., 2012; Cai et al., 2014; Wang et al., 1997), are higher than the $\delta^{34}S$ values of the polymetallic vein deposit. The possibility that oil-field brine only provided hydrosulfide (organic substances only in trace amounts) to the ore-forming process in the formation of the polymetallic vein deposits, can also be discounted.

Due to the fact that no marine evaporites or carbonates have been found in the host rock of our studied deposits and no organic matter has been reported in these ores, it is suggested that the relatively high $\delta^{34}S$ values were inherited from the ascending hydrothermal fluids. Sulfides in the polymetallic vein deposits are more enriched in ^{34}S than ordinary igneous rocks, which may controlled by magma-hydrothermal fluids assimilating higher $\delta^{34}S$ value minerals during upward migration (Leng et al., 2015), or the magma chamber underwent significant degassing of SO_2 (Zheng, 1990).

Uranium and thorium concentrations in the sulfides are too low to influence their lead isotopic compositions. Unlike basements rocks and the MVT deposits in this region, sulfides from the polymetallic vein deposits have homogeneous and low radiogenic lead isotope values. In the diagrams of $^{207}Pb/^{204}Pb$ vs. $^{206}Pb/^{204}Pb$ and $^{208}Pb/^{204}Pb$ vs. $^{206}Pb/^{204}Pb$ (Fig. 14), and when comparing to lead evolution curve (Zartman and Doe, 1981), it can be shown that all the sulfide samples from the polymetallic deposits plot between the orogenic and mantle lead curves. Samples from unaltered folded rocks (Liu and Zhu, 1994; Liang, 1989) are scattered in these diagrams but do not overlap with the fields of polymetallic vein-type deposits (Fig. 14). Samples from the MVT deposits (Schneider et al., 2002; Ye et al., 2012; Cai et al., 2014) plot close to or above the upper crust lead evolution curve, and show a positive correlations in diagrams of $^{207}Pb/^{204}Pb$ vs. $^{206}Pb/^{204}Pb$ and $^{208}Pb/^{204}Pb$ vs. $^{206}Pb/^{204}Pb$. These samples also do not overlap with the fields of polymetallic vein deposits. Moreover, lead isotopic compositions of altered basement rocks tend to show a shift towards the fields of the polymetallic deposits. This suggests that the basement rocks provided very little, if any, metals to these vein-type ores which have a different Pb source to MVT deposits in this region.

The low μ values (μ = 9.30–9.42) and highly homogeneous Pb isotopic compositions of the polymetallic vein deposits are similar to those commonly found in orogenic mineral systems, which contain a considerable contribution from the mantle or in deeper basement rocks in the continental crustal infrastructure (Doe and Zartman, 1982). Thus, it is inferred that the metals of polymetallic vein Zn-Pb deposits were sourced from a mixed mantle and crust source, and the metalliferous fluids were homogenized before their arrival at the sites of sulfide deposition.

Indium is highly dispersed in the Earth's crust and occurs in very low concentrations, with a crustal average concentration of 0.05 ppm (Tu, 2002; Taylor and McLennan, 1985; Schwarz-Schampera and Herzig, 2002). It is a highly volatile chalcophile element in magmatic processes (Schwarz-Schampera and Herzig, 2002) and is transported in high temperature gases of active magmatic systems (Kovalenker et al., 1993; Wahrenberger et al., 2002; Seifert and Sandmann, 2006; Zhang et al., 1998). Sphalerite that crystallized from the Kudryavyi volcano (Iturup Island, Russia) has indium concentrations of about 14.9 wt% (Kovalenker et al., 1993), and the dominant indium-bearing phases are gaseous species such as InCl, $InCl_3$ and InBr (Wahrenberger et al., 2002). Seward et al. (2000) considered the main forms of indium transport in hydrothermal fluids to include: indium chloride complexes and hydrolyzed species ($InCl_4^-$ and $InClOH^-$). Mineralization of In dominantly occurs predominantly in magmatic related deposits (86%), such as volcanic-hosted massive sulfide deposits, epithermal deposits, polymetallic vein-type base metal deposits, granite-related tin-base metal deposits and skarn deposits; as well as sedimentary exhalative deposits (13%) (Schwarz-Schampera and Herzig, 2002; Cook et al., 2009; Dill et al., 2013). Bulk In concentrations in sphalerite range from 1.64 ppm to 36.00 ppm (n = 12, mean = 12.90 ppm), while concentrations in sphalerite range from 4.77 ppm to 189.50 ppm (n = 26, mean = 46.49 ppm). The combined evidence of H-C-O-Pb isotopic composition, which record a magmatic hydrothermal character, the relatively higher indium concentrations in bulk ore and sphalerite compared to MVT deposits, as well as vein-like, fault-bounded mineralization, suggests a magmatic hydrothermal origin of the polymetallic vein-type deposits.

6.4. Genetic model for the polymetallic vein-type Zn-Pb deposits in the northwestern margin of Jiangnan Orogen

As mentioned above, besides a few Caledonian lamproites, no other magmatic events could be observed in this region, especially around the polymetallic vein Zn-Pb deposits. Therefore, it is difficult to directly link Zn-Pb mineralization to magmatism. However, some clues seem to suggest that: (1) A series of ca. 400–464 Ma (peaking at ca. 420–446 Ma) and ca. 220–233 Ma granites (such as the Baimashan and Yuechenlin Plutons) were emplaced into the eastern Jiangnan Orogen in response to crust thickening during the Caledonian (Silurian to Middle Devonian) and Indosinian intracontinental orogeny (Permian to Middle Triassic) (Wang et al., 2012, 2013; Yang et al., 2014; Wu et al., 2012; Chen et al., 2013; Zhang et al., 2013); (2) Geophysical data does reveal the presence of various dome-shaped structures and residual gravity anomalies at depth in this area (Wang et al., 2011; Yang et al., 2014), and the gravity anomalies are parallel to the distribution trends of the polymetallic veins and major faults. Thus, considering the huge thickness of sedimentary rocks deposited since the Neoproterozoic in this area, such as the 7 km thick Banxi Group, it is likely that concealed plutons corresponding to these two periods do exist at depth.

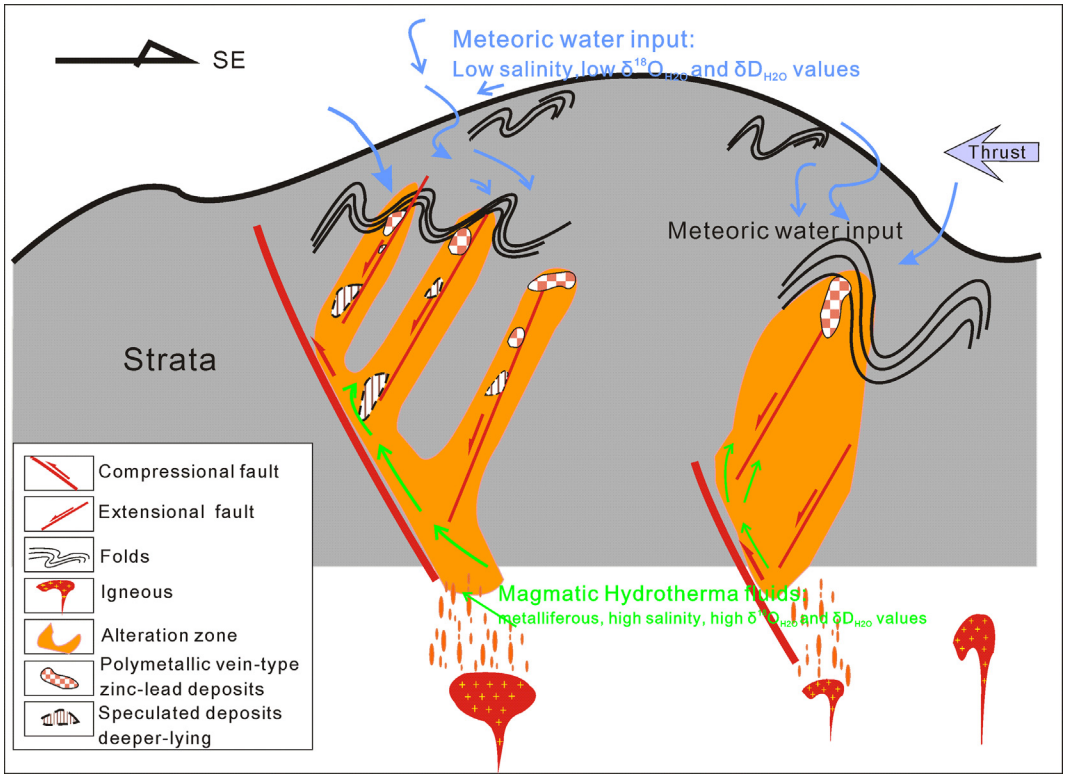

Fig. 15. Schematic diagram illustrating the genetic model of the zinc-lead polymetallic vein deposits in Xiangxi-Qiandong metallogenic belt. Long oval indicates concentration and degassing of magmatic-hydrothermal fluids and metals from an igneous source. Small arrows indicate meteoric water input into dilatant structures and mixed with magmatic hydrothermal fluid, resulting in the deposition of sulfides in veins and breccia.

The challenge in providing further understanding of genetic model of the polymetallic vein deposits is the lack of precise dating to constrain the mineralization age. Along the northwest margin of the Jiangnan Orogen, multiple paleo-Caledonian mineralization events have been recognized: 400–412 Ma quartz–vein type gold deposits (Re-Os dating for arsenopyrite, Wang et al., 2011), 410 Ma Shizishan MVT Zn-Pb deposit (Rb-Sr age of Sphalerite, Duan et al., 2014). Hu et al. (2010) used the K-Ar method on illite in slate of the Banxi Group to confine the Caledonian tectono-thermal event in the northwest margin of Jiangnan Orogen to 419–389 Ma. This tectono-thermal event age corresponds to a 425 Ma fission track age of zircon selected from the host rock of the polymetallic vein deposits (our unpublished data) suggesting that the Caledonian tectono-thermal event was intense in this region. The mineralization age of the polymetallic deposits is likely related to this tectono-thermal event, and it also seems that the polymetallic vein-type and MVT Zn-Pb deposits are contemporaneous. Both were mineralized to the background of the Guangxi Orogeny. However, the ore texture, sulfide minerals assemblage, elemental association and isotopic compositions of sulfides and/or carbonates are significantly different between the two deposits. Also, any intense post-ore alteration textures have been found in both the MVT and/or polymetallic vein Zn-Pb deposit, thus ruling out the possibility of remobilization of one ore to form the other.

Consequently, a simplified genetic model for the polymetallic vein deposits is proposed for the northwestern margin of the Jiangnan Orogen (Fig. 15). First, intracontinental orogenic events resulted in the crustal thickening and numerous granite intrusions (Charvet et al., 2010; Wang et al., 2012; Zhang et al., 2013). Next, incompatible elements such as zinc, lead, cadmium, indium and copper, became concentrated in hydrothermal fluids derived from magma degassing (Sinclair et al., 2006). These highly saline magmatic hydrothermal fluids with high $\delta^{18}O_{H2O}$ and δD_{H2O} upwelled along faults and breccia zones of surrounding country rocks. As they filled these dilatant structures and/or mixed with diluted meteoric water (low salinity, low $\delta^{18}O_{H2O}$ and δD_{H2O}), it caused the deposition of sulfides and associated minerals (Figs. 2 and 4, Fig. 5a–f).

This model is similar to mechanisms proposed for other indium-bearing polymetallic vein-type base metal deposits (Sinclair et al., 2006; Schwarz-Schampera and Herzig, 2002). Generally, indium-bearing polymetallic deposits are also likely enriched in Sn, Cu and Ag (Sinclair et al., 2006; Schwarz-Schampera and Herzig, 2002; Seifert and Sandmann, 2006; Shimizu and Kato, 1991; Zhang et al., 1998; Dill et al., 2013). Amongst others and beneath these polymetallic vein deposits, there is also a great potential to trace deeper-lying sulfide ores and higher temperature deposits (such as Zn, Pb, Cu and Sn mineralization).

7. Conclusions and implications

1) The ore-forming processes of polymetallic vein Zn-Pb deposits are different from those of MVT Zn-Pb deposits along the XQMB. Hydrogen, oxygen, and carbon isotopic data of the ores indicate that the ore-forming fluids were derived from a magmatic-hydrothermal system and became mixed with meteoric water. This accord with other evidence from ore-bound fluid inclusions, which shows that ore-forming processes were related to input of relatively low salinity fluids. Whereas the sulfur isotope compositions do not preclude the possibility of a non-magmatic fluid contribution. Homogeneous and unradiogenic lead isotopic compositions of sulfides indicate a mixed source of metals from both the mantle and crust.

2) The XQMB, located at the central part of the low-temperature metallogenic district in South China, which contains Au, Hg, As, Sb, Pb-Zn, Ni-Mo-PGE, U, P, barite and dispersed elements deposits with area more than 0.5 million km^2 (Tu, 2002; Hu et al., 2002; Hu and Zhou, 2012). Mineralization in this outstanding metallogenic district was primarily controlled by magmatism, as suggested by Zhou et al. (2001), Peng and Frei (2004), Wen and Carignan (2011), Wen et al. (2016) and Zhu et al. (2016) or relates to basinal brines that leached ore-forming materials from low metamorphic clastic series and limestone rocks of the Neoproterozoic to Phanerozoic (Tu, 2002; Hu et al., 2002; Peng et al., 2003; Ye et al., 2012; Gu et al., 2012; Chen et al., 2014).

The polymetallic vein Zn-Pb deposits, located at the junction of Yangtze Block and Jiangnan Orogen, are mostly likely explained by a model of magmatic hydrothermal fluid channeled along faults and breccia zones of the northwestern Jiangnan Orogen and mixing with diluted meteoric water. This model provides a new perspective on the mineralization processes in the low temperature metallogenic district of South China. Under the large thickness of covering rocks, concealed magmatic plutons may exist that were involved in metallogenesis of at least part of the low-temperature sediment-hosted deposits.

Acknowledgements

This project was financially supported by 973 Program (2014CB440904), the strategic Priority Research Program (B) of Chinese Academy of Sciences (Grant No. XDB18000000) and CAS/SAFEA International Partnership Program for Creative Research Teams (KZZD-EW-TZ-20).

Appendix A. Supplementary data

Supplementary data associated with this article can be found, in the online version, at http://dx.doi.org/10.1016/j.oregeorev.2017.03.022.

References

Barton, P.B., Bethke, P.M., 1987. Chalcopyrite disease in sphalerite: pathology and epidemiology. Am. Mineral. 72, 451–467.
Beaty, D.W., Cunningham, C.G., Rye, R.O., Steven, T.A., Gonzalez-Urien, E., 1986. Geology and geochemistry of the Deer Trail Pb-Zn-Ag-Au-Cu manto deposits, Marysvale district, west-central Utah. Econ. Geol. 81 (8), 1932–1952.
Bodnar, R.J., 1993. Revised equation and table for determining the freezing-point depression of H_2O-NaCl solutions. Geochim. Cosmochim. Acta 57 (3), 683–684.
Burke, E.A.J., 2001. Raman microspectrometry of fluid inclusions. Lithos 55 (s 1–4), 139–158.
Cai, C.F., Worden, R.H., Bottrell, S.H., Wang, L.S., Yang, C.C., 2003. Thermochemical sulphate reduction and the generation of hydrogen sulphide and thiols (mercaptans) in Triassic carbonate reservoirs from the Sichuan Basin, China. Chem. Geol. 202 (1), 39–57.
Charvet, J., Shu, L., Faure, M., Choulet, F., Wang, B., Lu, H., Breton, N.L., 2010. Structural development of the lower paleozoic belt of South China: genesis of an intracontinental orogen. J. Asian Earth Sci. 39 (4), 309–330.
Cai, Y.X., Yang, H.M., Duan, R.C., Lu, S.S., Zhang, L.G., Liu, C.P., Qiu, X.F., 2014. Fluid Inclusions and S, Pb, C isotope geochemistry of Pb-Zn deposits hosted by lower Cambrian in western Hunan- eastern Guizhou Area. Geoscience 28 (1), 29–41 (in Chinese with English abstract).
Chen, D., Wang, J., Qing, H., Yan, D., Li, R., 2009. Hydrothermal venting activities in the early Cambrian, South China: petrological, geochronological and stable isotopic constraints. Chem. Geol. 258 (3–4), 168–181.
Chen, S.B., Fu, J.M., Ma, L.Y., Jiang, G.X., Chen, X.Q., Lu, Y.Y., Tong, X.R., 2013. Indosinian metallogentic activity in Yuechengling-Miaoershan area, northeastern Guangxi: implications from zircon U-Pb ages and Hf isotopic constraint on ore-forming granites in Youmaling and Jiepai deposits. Geol. China 40 (4), 1189–1201 (in Chinese with English abstract).
Chen, M., Zhang, Z., Santosh, M., Dang, Y., Zhang, W., 2014. The Carlin-type gold deposits of the "golden triangle" of SW China: Pb and S isotopic constraints for the ore genesis. J. Asian Earth Sci. 103 (1), 115–128.
Chen, X., Zhang, Y.D., Fan, J.X., Chen, X.Q., Lu, Y.Y., Tong, X.R., 2010. Ordovician graptolite-bearing strata in southern Jiangxi with a special reference to the Kwangsian Orogeny. Sci. China: Earth Sci. 53, 1602–1610. http://dx.doi.org/10.1007/s11430-010-4117-6.
Chen, X., Zhang, Y.G., Fan, J.X., Tang, L., Sun, H.Q., 2012. Onset of the Kwangsian Orogeny as evidenced by biofacies and lithofacies. Sci. China: Earth Sci. 55, 1592–1600. http://dx.doi.org/10.1007/s11430-012-4490-4.
Chu, X.L., 2004. Snow ball earth during the Neoproterozoic. Bull. Mineralgy Petrol. Geochem. 23 (3), 233–238 (in Chinese).
Clayton, R.N., Mayeda, T.K., 1963. The use of bromine pentafluoride in the extraction of oxygen from oxides and silicates for isotopic analysis. Geochim. Cosmochim. Acta 27 (1), 43–52.
Clayton, R.N., O'Neil, J.R., Mayeda, T.K., 1972. Oxygen isotope exchange between quartz and water. J. Geophys. Res. Atmos. 77 (17), 3057–3067.
Coleman, M.L., Shepherd, T.J., Durham, J.J., Rouse, J.E., Moore, G.R., 1982. Reduction of water with zinc for hydrogen isotope analysis. Anal. Chem. 54 (6), 993–995.
Cook, N.J., Ciobanu, C.L., Pring, A., Skinner, W., Shimizu, M., Danyushevsky, L., Saini-Eidukat, B., Melcher, F., 2009. Trace and minor elements in sphalerite: a LA-ICPMS study. Geochim. Cosmochim. Acta 73, 4761–4791. http://dx.doi.org/10.1016/j.gca.2009.05.045.
Deen, J.A., Rye, R.O., Munoz, J.L., Drexler, J.W., 1994. The magmatic hydrothermal system at Julcani, Peru; evidence from fluid inclusions and hydrogen and oxygen isotopes. Econ. Geol. 89 (8), 1924–1938.
Doe, B.R., Zartman, R.E., 1982. Plumbotectonics of Japan: some evidence for a rejuvenated craton. Mining Geology 32 (4), 285–289.
Duan, Q.F., Gao, L., Zeng, J.K., Zhou, Y., Tang, Z.Y., Li, K., 2014. Rb-Sr dating of sphalerite from Shizishan Pb-Zn deposit in Huayuan ore concentration area, westerm Hunan, and its geological significance. Earth Sci.-J. China Univ. Geosci. 39 (8), 977–999 (in Chinese with English abstract).
Dill, H.G., Garrido, M.M., Melcher, F., Gomez, M.C., Weber, B., Luna, L.I., Bahr, A., 2013. Sulfidic and non-sulfidic indium mineralization of the epithermal Au–Cu–Zn–Pb–Ag deposit Aan Roque (Provincia Rio Negro, SE Argentina) -with special reference to the "indium window" in zinc sulfide. Ore Geol. Rev. 51, 103–128.
Eldridge, C.S., Bourcier, W.L., Ohmoto, H., Barnes, H.L., 1988. Hydrothermal inoculation and incubation of the chalcopyrite disease in sphalerite. Econ. Geol. 83 (5), 978–989.
Fang, W.X., Hu, R.Z., Su, W.C., Qi, L., Xiao, J.F., Qi, L., Jiang, G.H., 2002. On intrusive ages of lamproites in Zhengyuan area, Guizhou Provience, China. Chin Sci. Bull. 47 (4), 307–312 (in Chinese).
Friedman, L., O'Neil, J.R., 1977. Compilation of stable isotope fractionation factors of geochemical interest. In: Fleischer, M., (Ed.), sixth ed., Data of geochemistry, Geological Survey Professional Paper, Reston, VA, vol. 440-KK, pp. KK1-KK12.
Geng, Y.S., 2015. The South China Craton. In: Zhai, M.G. (Ed.), Precambrian Geology of China. Springer-Verlag, Berlin, pp. 207–263. http://dx.doi.org/10.1007/978-3-662-47885-1.
Goldfard, R.J., Ayuso, R., Miller, M.L., Ebert, S.W., Marsh, E.E., Petsel, S.A., Miller, L.D., Bradley, D., Johnson, C., McClelland, W., 2004. The late Cretaceous Donlin Creek Gold deposit, southwestern Alaska: controls on Epizonal Ore formation. Econ. Geol. 99, 643–671.
Gu, X.X., Zhang, Y.M., Li, B.H., Dong, S.Y., Xue, C.J., Fu, S.H., 2012. Hydrocarbon- and ore-bearing basinal fluids: a possible link between gold mineralization and hydrocarbon accumulation in the Youjiang basin, South China. Miner. Deposita 47 (6), 663–682.
Hoefs, J., 2009. Stable Isotope Geochemistry. Springer-Verlag, Berlin.
Hu, R.Z., Su, W.C., Bi, X.W., Tu, G.Z., Hofstra, A.H., 2002. Geology and geochemistry of Carlin-type gold deposits in China. Miner. Deposita 37 (3–4), 378–392.
Hu, R.Z., Zhou, M.F., 2012. Multiple mesozoic mineralization events in South China – an introduction to the thematic issue. Miner. Deposita 47 (6), 579–588.
Hu, S.Q., Zhu, G., Zhang, B.L., Zhang, L., 2010. K-Ar geochronology of the Caledonian event in the Xufeng uplift. Geol. Rev. 56 (4), 490–500 (in Chinese with English abstract).
Huang, J., Chu, X.L., Jiang, G.Q., Feng, L.J., Chang, H.J., 2011. Hydrothermal origin of elevated iron, manganese and redox-sensitive trace elements in the ca. 635 Ma doushantuo cap carbonate. J. Geol. Soc. 168 (3), 805–816.
Huang, J., Chum, X.L., Zhang, Q.R., Feng, L.J., 2007. Constraints on the age of Neoproterozoic global glaciations. Earth Sci. Front. 14 (2), 249–256 (in Chinese with English abstract).
Jiang, G.Q., Kennedy, M.J., Nicholas, C.B., 2003. Stable isotopic evidence for methane seeps in Neoproterozoic postglacial cap carbonates. Nature 426 (6968), 822–826.
Kelly, W.C., Rye, R.O., Kelly, W.C., Rye, R.O., 1979. Geologic, fluid inclusion, and stable isotope studies of the Tin-Tungsten deposits of Panasqueira, Portugal. Econ. Geol. 74 (8), 1721–1822.
Kovalenker, V.A., Laputina, I.P., Znamenskii, V.S., Zotov, I.A., 1993. Indium mineralization of the Great Kuril Island Arc. Geol. Ore Deposits 35, 491–495.
Leach, D.L., Sangster, D.F., Kelley, K.D., Large, R.R., Garven, G., Allen, C.R., Gutzmer, J., 2005. Sediment-hosted lead-zinc deposit: a global perspective. Econ. Geol. 100 (Anniversary Volume), 561–607.
Leng, C.B., Zhang, X.C., Huang, Z.L., Huang, Q.Y., Wang, S.X., Ma, D.Y., Luo, T.Y., Li, C., Li, W.B., 2015. Geology, Re-Os ages, sulfur and lead isotopes of the Diyanqinamu porphyry Mo deposit, Inner Mongolia, NE China. Econ. Geol. 110 (2), 557–574.
Li, H.M., Zhang, C.Q., 2012. The Genetic Relationship between the H_2S-bearing gas in Sichuan Basin and Lead-Zinc-Copper Deposits around the Basin. Geol. Rev. 58 (3), 495–510 (in Chinese with English abstract).
Li, K., Wu, C.X., Tang, C.Y., Duan, Q.F., Yu, Y.S., 2014. Carbon and oxygen isotopes of Pb-Zn deposits in western Hunan and eastern Guizhou provinces and their

implications for the ore-forming process. Geol. China 41 (5), 1608–1619 (in Chinese with English abstract).
Li, X.H., Li, W.X., He, B., 2012. Building of the South China Block and its relevance to assembly and breakup of Rodinia supercontinent: observations, interpretations and test. Bull. Mineralogy Petrol. Geochem. 31, 543–559 (in Chinese with English abstract).
Li, X.H., Li, Z.X., Ge, W., Zhou, H., Li, W.X., Liu, Y., Michael, T.D.W., 2003. Neoproterozoic granitoids in South China: crustal melting above a mantle plume at ca. 825 Ma? Precambr. Res. 122 (s 1–4), 45–83.
Li, Z.X., Li, X.H., Kinny, P.D., Wang, J., 1999. The breakup of Rodinia: did it start with a mantle plume beneath South China? Earth Planet. Sci. Lett. 173 (3), 171–181.
Liang, H.Y., 1989. Ore material sources of the Longshan gold-antimony deposit. Mineral Deposits 8 (4), 39–48. http://dx.doi.org/10.16111/j.0258-7106.1989.04005 (in Chinese).
Liu, H.C., Zhu, B.Q., 1994. Research on the age of Banxi Groups and Lengjiaxi Groups, western Hunan Provience. China Sci. Bull. 39 (2), 148–150 (in Chinese).
Liu, L., Pu, K.X., Wang, M.S., Shen, C.S., 2008. The geologic structure character and prospection of Jinbao lead-zinc field, Zhenyuan, Guizhou. Guizhou Geol. 25 (2), 99–105 (in Chinese).
Machel, H.G., Krouse, H.R., Sassen, R., 1995. Products and distinguishing criteria of bacterial and thermochemical sulfate reduction. Appl. Geochem. 10 (4), 373–389.
Mao, J.W., Lehmann, B., Du, A.D., Zhang, G.D., Ma, D.S., Wang, Y.T., Zeng, M.G., 2002. Re-Os dating of polymetallic Ni-Mo-PGE-Au mineralization in lower Cambrian black shales of South China and its geologic significance. Econ. Geol. 97 (5), 1051–1061.
Mei, H.J., Tang, C.J., Li, S.R., Li, Y.M., Zhang, X.C., Lu, D.R., Zhang, L.C., 1998. Lamproites and kimberlites in China and the genesis of diamond deposit. Sci. China 41 (1), 54–92.
Moldovanyi, E.P., Walter, L.M., Land, L.S., 1993. Strontium, Boron, Oxygen, and Hydrogen isotope geochemistry of brines from basal strata of the Gulf coast sedimentary basin, USA. Geochim. Cosmochim. Acta 57 (9), 2083–2099.
Ohmoto, H., 1972. Systematics of sulfur and carbon isotopes in hydrothermal ore deposits. Econ. Geol. 67 (5), 551–578.
Ohmoto, H., 1986. Stable isotope geochemistry of ore deposits. Rev. Mineral. Geochem. 16 (6), 491–559.
Peng, B., Frei, R., 2004. Nd-Sr-Pb isotopic constraints on metal and fluid sources in W-Sb-Au mineralization at Woxi and Liaojiaping (western Hunan, China). Miner. Deposita 39 (3), 313–327.
Peng, J.T., Hu, R.Z., Burnard, P.G., 2003. Samarium–neodymium isotope systematics of hydrothermal calcites from the Xikuangshan antimony deposit (Hunan, China): the potential of calcite as a geochronometer. Chem. Geol. 200 (s1–2), 129–136.
Robinson, B.W., Kusakabe, M., 1975. Quantitative preparation of sulfur dioxide for $^{32}S/^{34}S$ analyses from sulfides by combustion with cuprous oxide. Anal. Chem. 47 (7), 1179–1181.
Rye, R.O., 1993. The evolution of magmatic fluids in the epithermal environment: the stable isotope perspective. Econ. Geol. 88 (3), 733–752.
Schneider, J., Boni, M., Lapponi, F., Bechstadt, T., 2002. Carbonate-Hosted zinc-lead deposits in the lower Cambrian of Hunan, South China: A radiogenic (Pb, Sr) isotope study. Econ. Geol., 1815–1827
Schwarz-Schampera, U., Herzig, P.M., 2002. Indium: Geology, Mineralogy, and Economics. Springer-Verlag, Berlin.
Seifert, T., Sandmann, D., 2006. Mineralogy and geochemistry of indium-bearing polymetallic vein-type deposits: Implications for host minerals from the Freiberg district, Eastern Erzgebirge, Germany. Ore Geol. Rev. 28 (1), 1–31.
Seward, T.M., Henderson, C.M.B., Charnock, J.M., 2000. Indium (III) chloride complexing and solvation in hydrothermal solutions to 350 8C: an EXAFS study. Chem. Geol. 167, 117–127.
Shimizu, M., Kato, A., 1991. Roquesite-bearing tin ores from the Omodani, Akenobe, Fukoku, and Ikuno polymetallic vein-type deposits in the inner zone of Southwestern Japan. Can. Mineral. 29, 207–215.
Shu, L.S., 2012. An analysis of principal features of tectonic evolution in South China Block. Geol. Bull. China 31, 1035–1053 (in Chinese with English abstract).
Sinclair, W.D., Kooiman, G.J.A., Martin, D.A., Kjarsgaard, I.M., 2006. Geology, geochemistry and mineralogy of indium resources at Mount Pleasant, New Brunswick, Canada. Ore Geol. Rev. 28 (1), 123–145.
Spangenberg, J., Fontbote, L., Sharp, Z.D., Hunziker, J., 1996. Carbon and oxygen isotope study of hydrothermal carbonates in the Zinc-Lead deposits of the San Vicente district, central Peru: a quantitative modeling on mixing processes and CO2 degassing. Chem. Geol. 133 (s1–4), 289–315.
Suchecki, R.K., Land, L.S., 1983. Isotopic geochemistry of burial-metamorphosed volcanogenic sediments, great valley sequence, northern California. Geochim. Cosmochim. Acta 47 (83), 1487–1499.
Tang, Z.Y., Deng, F., Li, K., Zhao, W.Q., Jin, S.C., 2013. Lithofacies palaeogeography of the Qingxudong epoch, Duyun stage, Cambrian period and its relationship to lead-zinc deposits in western Hunan and eastern Guizhou province. Geol. Explor. 49 (1), 19–27 (in Chinese with English abstract).
Taylor, H.P., 1997. Oxygen and hydrogen isotope relationships in hydrothermal mineral deposits. In: Barnes, H.L. (Ed.), Geochemistry of Hydrothermal Ore Deposits. Wileym New York, pp. 229–302.
Taylor, S.R., Mclennan, S.M., 1985. The Continental Crust: Its Composition and Evolution, An Examination of the Geochemical Record Preserved in Sedimentary Rocks. Blackwell Scientific Pub., p. 1985.
Tu, G.C., 2002. Two unique mineralization areas in southwest China. Bull. Mineralgy Petrol. Geochem. 21 (1), 1–2 (in Chinese).
Wahrenberger, C., Seward, T.M., Dietrich, V., 2002. Volatile traceelement transport in high-temperature gases from Kudriavy volcano (Iturup, Kurile Islands, Russia). In: Hellmann, R., Wood, A.W. (Eds.), Water-Rock Interactions, Ore Deposits, and Environmental Geochemistry: A Tribute to David A. Crerar, vol. 7. The Geochemical Society Special Publication, pp. 307–327.
Wang, H.Y., Shi, J.X., 1997. Sources of ore-forming materials and controls over depositional differentiation in the epithermal mineralization series in the Danzhai-Sandu-Duyun area of Guizhou province. Acta Mineral Sin. 17, 491–500 (in Chinese with English abstract).
Wang, J.S., Wen, H.J., Li, C., Ding, W., Zhang, J.R., 2011. Re-Os isotope dating of arsenopyrite from the quartz vein-type gold deposit, Southeastern Guizhou province, and its geological implications. Acta Geol. Sin. 85 (6), 955–964 (in Chinese with English abstract).
Wang, X.L., Zhao, G.C., Zhou, J.C., Liu, Y.S., Hu, J., 2008. Geochronology and Hf isotopes of zircon from volcanic rocks of the Shuangqiaoshan Group, South China: implications for the Neoproterozoic tectonic evolution of the eastern Jiangnan Orogen. Gondwana Res. 14, 355–367.
Wang, X.L., Zhou, J.C., Qiu, J.S., Gao, J.F., 2004. Geochemistry of the Meso- to Neoproterozoic basic-acid rocks from Hunan province, South China: implications for the evolution of the western Jiangnan Orogen. Precambr. Res. 135, 79–103.
Wang, Y.J., Fan, W.M., Zhang, G.W., Zhang, Y.H., 2013. Phanerozoic tectonics of the South China Block: key observations and controversies. Gondwana Res. 23 (4), 1273–1305.
Wang, Y.J., Wu, C.M., Zhang, A.M., Fan, W.M., Zhang, Y.H., Zhang, Y.Z., Peng, T.P., Yin, C.Q., 2012. Kwangsian and Indosinian reworking of the eastern South China Block: Constraints on zircon U-Pb geochronology and metamorphism of amphibolites and granulites. Lithos 150, 227–242. http://dx.doi.org/10.1016/j.lithos.2012.04.022.
Wen, H.J., Carignan, J., Zhang, Y.X., Fan, H.F., Cloquet, C., Liu, S.R., 2011. Molybdenum isotopic records across the Precambrian-Cambrian boundary. Geology 39 (8), 775–778.
Wen, H.J., Carignan, J., 2011. Selenium isotopes trace the source and redox processes in the black shale-hosted Se-rich deposits in China. Geochim. Cosmochim. Acta 75 (6), 1411–1427.
Wen, H.J., Zhu, C.W., Zhang, Y.X., Cloquet, C., Fan, H.F., Fu, S.H., 2016. Zn/Cd ratios and cadmium isotope evidence for the classification of lead-zinc deposits. Sci. Rep. 6, 25273. http://dx.doi.org/10.1038/srep25273.
Wilkinson, J.J., 2001. Fluid inclusions in hydrothermal ore deposits. Lithos 55 (1–4), 229–272.
Wu, J., Liang, H.Y., Huang, W.T., Wang, C.L., Sun, W.D., Sun, Y.L., Li, J., Mo, J.H., Wang, X.Z., 2012. Indosinian isotope ages of plutons and deposits in southwestern Miaoershan-Yuechengling, northeastern Guangxi and implications on Indosinian mineralization in South China. China Sci. Bull. 57, 1024–1035. http://dx.doi.org/10.1007/s11434-011-4968-z.
Wu, Y., Zhang, C.Q., Mao, J.W., OuYang, H.G., Sun, J., 2013. The genetic relationship between hydrocarbon systems and Mississippi Valley-type Zn–Pb deposits along the SW margin of Sichuan Basin, China. Int. Geol. Rev. 55 (8), 941–957.
Yang, Z., Wang, R.C., Zhang, W.L., Chu, Z.Y., Chen, J., Zhu, J.C., Zhang, R.Q., 2014. Skarn-type tungsten mineralization associated with the Caledonian (Silurian) Niutangjie granite, northern Guangxi, China. Sci. China: Earth Sci. 57, 1551–1566. http://dx.doi.org/10.1007/s11430-014-4838-z.
Yang, Z.W., Liu, L., Liao, L.P., Qin, C.J., Wen, H.J., 2015. Discussion on stable isotope characteristics and the source of mineral material in the Jinbao lead-zinc deposit in Zhenyuan County, Southeastern Guizhou province, China. Acta Mineral. Sin. 35 (2), 147–153 (in Chinese with English abstract).
Yao, J., Shu, L., Santosh, M., Li, J., 2012. Precambrian crustal evolution of the South China block and its relation to supercontinent history: constraints from U-Pb ages, Lu-Hf isotopes and REE geochemistry of zircons from sandstones and granodiorite. Precambr. Res. 208–211, 19–48.
Ye, L., Cook, N.J., Ciobanu, C.L., Liu, Y.P., Zhang, Q., Liu, T.G., Gao, W., Yang, Y.L., Danyushevsky, L., 2011. Trace and minor elements in sphalerite from base metal deposits in South China: a LA-ICPMS study. Ore Geol. Rev. 39, 188–217. http://dx.doi.org/10.1016/j.oregeorev.2011.03.001.
Ye, L., Cook, N.J., Liu, T.G., Ciobanu, C.L., Gao, W., Yang, Y., 2012. The Niujiaotang Cd-rich zinc deposit, Duyun, Guizhou province, Southwest China: ore genesis and mechanisms of cadmium concentration. Miner. Deposita 47 (6), 1–18.
Ye, L., Pan, Z.P., Li, C.Y., Liu, T.G., Xia, B., 2005. Isotopic geochemical characters in Niujiaotang Cd rich zinc deposit, Duyun, Guizhou. J. Mineralogy Petrol. 25 (2), 70–74 (in Chinese with English abstract).
Yeh, H.W., 1980. D/H ratios and late-stage dehydration of shales during burial. Geochim. Cosmochim. Acta 44 (2), 341–352.
Yin, C.Y., Liu, D.Y., Gao, L.Z., Wang, Z.Q., Xing, Y.S., Jiang, P., Shi, Y.R., 2003. Lower boundary age of the Nanhua Syatem and the Gucheng glacial stage: evidence from SHRIMP II dating. China Sci. Bull. 48 (16), 1657–1662.
Yue, C.H., Yang, G.S., 1993. The geological features and prospecting of Pb-Zn deposits in Zhenyuan and Taijiang regions, Guizhou. Guizhou Geol. 1 (1), 76–81 (in Chinese).
Zartman, R.E., Doe, B.R., 1981. Plumbotectonics—the model. Tectonophysics 75, 135–162.
Zhai, M.G., 2013. The main old lands in China and assembly of Chinese unified continent. Sci China: Earth Sci. 56, 1829–1852. http://dx.doi.org/10.1007/s11430-013-4665-7.
Zhang, G.W., Guo, A.L., Wang, Y.J., Li, S.Z., Dong, Y.P., Liu, S.F., He, D.F., Cheng, S.Y., Lu, R.K., Yao, A.P., 2013. Tectonics of South China Continent and its implications. Sci. China Earth Sci. 56 (11), 1804–1828.

Zhang, Q., Zhan, X.Z., Pan, J.Y., Shao, S.X., 1998. Geochemical enrichment and mineralization of indium. Chin. J. Geochem. 17 (3), 221–225.
Zhang, Q.R., Chu, X.L., Feng, L.J., 2009. Discussion on the Neoproterozoic glaciations in the South China Block and their related paleolatitudes. China Sci. Bull. 54 (10), 1797–1800.
Zhang, S.H., Jiang, G.Q., Han, Y.G., 2008. The age of the Nantuo Formation and Nantuo glaciation in South China. Terra Nova 20 (4), 289–294.
Zhao, G.C., Cawood, P.A., 2012. Precanbrian geology of China. Precambrian Res. 222–223, 13–54.
Zheng, Y.F., 1990. The effect of Rayleigh degassing of magma on sulfur isotope composition: a quantitative evaluation. Terra Nova 2 (1), 74–78.
Zhou, C.M., Tucker, R., Xiao, S.H., Peng, Z.X., Yuan, X.L., Chen, Z., 2004. New constraints on the ages of Neoproterozoic glaciations in South China. Geology 32 (5), 437–440.
Zhou, C., Wei, C.S., Guo, J.Y., Li, C.Y., 2001. The source of metals in the Qilinchang Zn-Pb deposit, Northeastern Yunnan, China: Pb-Sr isotope constraints. Econ. Geol. 96 (3), 583–598.
Zhu, C.W., Wen, H.J., Zhang, Y.X., Fan, H.F., 2016. Cadmium and sulfur isotopic compositions of the Tianbaoshan Zn–Pb–Cd deposit, Sichuan Province, China. Ore Geol. Rev. 72, 152–162.